AC SAF VALIDATION REPORT

Validated products:

Name	Satellite
Sulphur dioxide total ozone	MetOp-C

GOME2/MetopC SO$_2$ Pollution VCD
201902_201907 2019 | 0.25x0.25
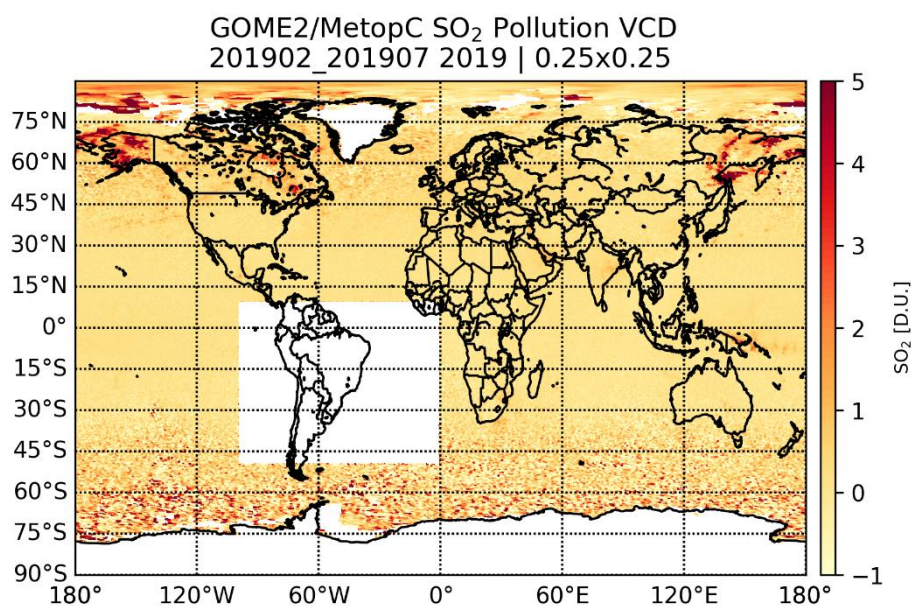
Average GOME2/MetopC sulphur dioxide polluted vertical column density between February and July 2019 on a 0.25x0.25° grid.

Authors:

Name	Institute
Mariliza Koukouli	Aristotle University of Thessaloniki
Gaia Pinardi	Royal Belgian Institute for Space Aeronomie
Nicolas Theys	Royal Belgian Institute for Space Aeronomie
Pascal Hedelt	German Aerospace Center

Reporting period: February 2019 – July 2019

Input data versions: GOME-2 L1b version 6.3

Data processor versions: GDP 4.9, UPAS version 1.4.0

Introduction to EUMETSAT Satellite Application Facility
on Atmospheric Composition monitoring (AC SAF)

Background

The monitoring of atmospheric chemistry is essential due to several human caused changes in the atmosphere, like global warming, loss of stratospheric ozone, increasing UV radiation, and pollution. Furthermore, the monitoring is used to react to the threats caused by the natural hazards as well as follow the effects of the international protocols.

Therefore, monitoring the chemical composition and radiation of the atmosphere is a very important duty for EUMETSAT and the target is to provide information for policy makers, scientists and general public.

Objectives

The main objectives of the AC SAF is to process, archive, validate and disseminate atmospheric composition products (O_3, NO_2, SO_2, BrO, HCHO, H_2O, OClO, CO, NH3), aerosol products and surface ultraviolet radiation products utilising the satellites of EUMETSAT. The majority of the AC SAF products are based on data from the GOME-2 and IASI instruments onboard Metop satellites.

Another important task besides the near real-time (NRT) and offline data dissemination is the provision of long-term, high-quality atmospheric composition products resulting from reprocessing activities.

Product categories, timeliness and dissemination

NRT products are available in less than three hours after measurement. These products are disseminated via EUMETCast, WMO GTS or internet.

- Near real-time trace gas columns (total and tropospheric O_3 and NO_2, total SO_2, total HCHO, CO) and high-resolution ozone profiles
- Near real-time absorbing aerosol indexes from main science channels and polarization measurement detectors
- Near real-time UV indexes, clear-sky and cloud-corrected

Offline products are available within two weeks after measurement and disseminated via dedicated web services at EUMETSAT and AC SAF.

- Offline trace gas columns (total and tropospheric O_3 and NO_2, total SO_2, total BrO, total HCHO, total H_2O) and high-resolution ozone profiles
- Offline absorbing aerosol indexes from main science channels and polarization measurement detectors
- Offline surface UV, daily doses and daily maximum values with several weighting functions

Data records are available after reprocessing activities from the EUMETSAT Data Centre and/or the AC SAF archives.

- Data records generated in reprocessing
- Lambertian-equivalent reflectivity
- Total OClO

Users can access the AC SAF offline products and data records (free of charge) by registering at the AC SAF web site.

More information about the AC SAF project, products and services: https://acsaf.org/

AC SAF Helpdesk: helpdesk@acsaf.org

Twitter: https://twitter.com/Atmospheric_SAF

TABLE OF CONTENTS

TABLE OF FIGURES

TABLE OF SUPPLEMENT FIGURES

TABLE OF TABLES

ACRONYMS AND ABBREVIATIONS

AMF	Air Mass Factor
AUTH	Aristotle University of Thessaloniki
BIRA	Royal Belgian Institute for Space Aeronomie
BUFR	Binary Universal Form for the Representation of meteorological data
CDOP	Continues Development and Operations Proposal
CNRS/LATMOS	Laboratoire Atmosphère, Milieux, Observations Spatiales du CNRS
DLR	German Aerospace Centre
DOAS	Differential Optical Absorption Spectroscopy
Envisat	Environmental Satellite
ESA	European Space Agency
EUMETSAT	European Organisation for the Exploitation of Meteorological Satellites
GDP	GOME Data Processor
GOME	Global Ozone Monitoring Experiment
GOME2A	Second Global Ozone Monitoring Experiment (MetOp-A)
GOME2B	Second Global Ozone Monitoring Experiment (MetOp-B)
HDF5	Hierarchical Data Format
IASB	Institut d'Aéronomie Spatiale de Belgique
MetOp	Meteorological Operational satellite
NRT	Near-real-time
O3M-SAF	Ozone and Atmospheric Chemistry Monitoring Satellite Application Facility
OMI	Ozone Monitoring Instrument
SAOZ	Système d'Analyse par Observation Zénithale
SCD	Slant Column Density
SCIAMACHY	Scanning Imaging Absorption spectroMeter for Atmospheric CHartography
SNR	Signal to Noise Ratio
SO_2	Sulphur dioxide
SZA	Solar Zenith Angle
UPAS	Universal Processor for UV/VIS Atmospheric Spectrometers
UVVIS	ground-based DOAS ultraviolet-visible spectrometer
VCD	Vertical Column Density

EUMETSAT
AC SAF

REFERENCE: **SAF/AC/AUTH/VR/SO2**
ISSUE: 11/2020
DATE: 30/11/2010
PAGES: Page **9** of **62**

Applicable AC SAF Documents

[ATBD] Algorithm Theoretical Basis Document for GOME-2 Total Column Products of Ozone, NO_2, BrO, SO_2, H_2O, HCHO and Cloud Properties (GDP 4.9 for AC SAF OTO and NTO), SAF/AC/DLR/ATBD/01, 3/B Rev.1, Valks, P., et al., June 2019. https://acsaf.org/docs/atbd/Algorithm_Theoretical_Basis_Document_NTO_OTO_Nov_2019.pdf last accessed: 15.11.2020.

[PUM] Product User Manual for GOME-2 Total Column Products of Ozone, NO_2, BrO, SO_2, H_2O, HCHO, OCIO and Cloud Properties (GDP 4.9 for AC SAF OTO and NTO), SAF/AC/DLR/PUM/01, 3/B Rev.1, Valks, P., et. al., 2019. https://acsaf.org/docs/pum/Product_User_Manual_NTO_OTO_Nov_2019.pdf last accessed: 15.11.2020.

[PRD] Product Requirements Document, Issue 1.5, SAF/AC/FMI/RQ/PRD/001, Issue 1.5, D. Hovila, S. Hassinen, P. Valks, J., S. Kiemle, O. Tuinder, H. Joench-Soerensen, June 2019.

[VR] Validation Report, O3M SAF SO_2 GDP 4.8 VALIDATION REPORT, SAF/O3M/IASB/VR/SO2/112/TN-IASB-GOME-2-O3MSAF-SO2-2015, N. Theys, M Koukouli, G. Pinardi, M. Van Roozendael, D. Balis, P. Hedelt, and P. Valks, https://acsaf.org/docs/vr/Validation_Report_NTO_OTO_DR_SO2_GDP48_Dec_2015.pdf, last accessed: 19.11.2020.

Technical information

Satellite ID: M03~~1~~
Product type: O3MOTO
Validation reporting period   **February – July 2019**
Level-2 processor version   **GDP 4.9, UPAS version 1.4.0**

Input GOME-2/MetOp-C Level-1B data version table

Start Date	Start Orbit	Level 1B Version
February 1, 2019	01222	6.3.0

Acknowledgments

1 INTRODUCTION

Scope of this document

The present document reports on the validation of the offline GOME-2/MetOp-C between February and July 2019. The data are produced operationally by the GOME Data Processor (GDP) version 4.9 operated at DLR in the framework of the EUMETSAT Satellite Application Facility on Atmospheric Composition Monitoring (ACSAF). This report addresses the quality of individual components of the data processing, starting with new GDP4.9 algorithm settings. The report includes comparisons of GOME2 final data products with correlative observations from independent sources, namely, SO_2 columnar data produced with GDP versions 4.8, S5P/TROPOMI, OMI/Aura, MAX-DOAS and zenith sky ground-based observations.

Preliminary remarks

The aim of the present document is to report on the validation of the GOME2 SO_2 columns from MetOp-C (hereafter referred to as GOME2C) against various satellite data sets and ground-based data.

Reported validation studies were carried out at the Laboratory of Atmospheric Physics, Aristotle University of Thessaloniki (AUTH), the Belgian Institute for Space Aeronomy (IASB-BIRA, Brussels, Belgium) and at DLR Remote Sensing Technology Institute (DLR-IMF, Oberpfaffenhofen, Germany) in the framework of EUMETSAT Satellite Application Facility on Atmospheric Composition Monitoring (ACSAF).

Roadmap of this document

This document is divided in three main parts: in this section we give a brief description of the different GOME2/Metop algorithms, namely GDP4.8 and GDP4.9 [Section 1.1], and discuss the reasons for which we are not directly comparing either the resulting Slant Column or the Vertical Column Densities reported by the three GOME2 Metop instruments [Section 1.2]. Furthermore, we summarize the Product Requirements for the SO2 vertical column densities reported by the GOME2/MetopC instrument [Section 1.3.] In the second part, we discuss briefly the space-based data files that appear in this document, namely the GOME2C [Section 2.1], the S5P/TROPOMI [Section 2.2] and the OMI/Aura [Section 2.3] providing only the pertinent information necessary of this report for the different datasets. In the third, and larger part, we first include some further comparisons on the Slant Column Densities [SCDs], in Section 3.1, followed by the comparison of the GOME2C anthropogenic SO_2 product to OMI, TROPOMI and MAX-DOAS observations [Section 3.2] and the GOME2C volcanic SO_2 product to GOME2B, TROPOMI and zenith-sky ground-based observations [Section 3.3.] Summary and recommendations follow in the Conclusions section.

1.1   The GOME2/METOP GDP4.8 & GDP4.9 Algorithms

The GOME2/Metop-C (hereafter GOME2C) Sulphur Dioxide Column, SO_2, product has been processed with the DOAS algorithm version GDP4.9. The main differences between GDP4.8 [see ATBD], which is the previous operational algorithm used for the GOME-2/MetopA and MetopB

processing, and GDP4.9 concern the SO_2 vertical column retrieval. The main changes for the GOME2/MetopC GDP4.9 product are the following [DLR, personal communication]:

- **SO_2 absorption cross-section:**

The Bogumil et al., 2003, SO_2 absorption cross-section was changed to the Birk and Wagner, 2018, cross-sections, which were measured within the framework of the ESA project SEOM-IAS (Scientific Exploitation of Operational Missions - Improved Atmospheric Spectroscopy Databases), ESA/AO/1-7566/13/I-BG. Details on the project can be found at http://www.wdc.dlr.de/seom-ias/.

The reasoning behind this choice was that the Bogumil et al., 2003, cross-sections have been measured using the SCIAMACHY/Envisat Flight Module and always needed to be de-convolved and then re-convolved with the current instrument's slit function. Furthermore, the temperature dependence of the XS in the Bogumil dataset was partly non-linear. The new DLR SEOM-IAS dataset (Birk and Wagner, 2018) shows an up to 10% lower absorption in the wavelength range 310-326nm with respect to the Bogumil et al. (2003) for the reference temperature of 203K. The effect on the retrieved SO_2 SCDs was however found to be negligible while the RMS of the background is found to be slightly lower. This change in cross-section is performed for all three GOME2 instruments.

- **Fitting window:**

The wavelength range of the SO_2 fit window was slightly increased, from 315-326nm (GDP4.8) to 312-326nm (GDP4.9) to include the strong SO_2 line at 313 nm and to make the fit more stable. The new fit window range is now identical to the S5P/TROPOMI fit window range.

- **Detection flag:**

The volcano activity detection algorithm to identify elevated SO_2 values from volcanic eruptions implemented in GDP 4.8 was further improved (SO2_Volcano_Flag in the DETAILED_RESULTS/SO2 group). For MetOp-C a new flagging algorithm was implemented in the GDP 4.9 that is identical to the operational Sentinel-5P/TROPOMI SO_2 flagging algorithm, which is used to flag enhanced levels of SO_2 (sulfurdioxide_enhanced_detection_flag in the S5P files.) The main difference to the algorithm used for MetOp-A and –B is that it can distinguish between the source type of the enhanced SO_2 signal. The following table shows the values that can be found in the SO2_Volcano_Flag for MetOpC.

Table 1. The new Volcanic SO_2 Flags implemented in GOME2/MetopC L2 files.

Value	Volcanic_Flag for GOME-2 on MetOp-C
0	No detection
1	Enhanced SO_2 detection Pixel as well as >50% of the neighboring pixels exceed a threshold SO_2 value of 0.8 DU.

2	Enhanced SO_2 detection in the vicinity of a known volcano. Pixel as well as >50% of the neighboring pixels exceed a threshold SO_2 value of 0.5 DU.
3	Enhanced SO_2 detection in the vicinity of an anthropogenic source. Pixel as well as >50% of the neighboring pixels exceed a threshold SO_2 value of 2 DU.
4	Enhanced SO_2 detection in the SAA or for SZA>70deg Pixel as well as >66% of the neighboring pixels exceed a threshold SO_2 value of 3 DU in the South Atlantic Anomaly region (SAA, 60-100°S, 100-0°) or for SZA angles >70°

- **Various:**

For the analysis of the GOME2C observations, the slit function was optimized based on the existing slit function file and spectral observation. The changes in the slit function were small but led to an improvement of the DOAS fit. Another improvement was achieved by introducing a pseudo absorber for possible orbital variations of the resolution.

1.2 Level-1b issues affecting the GOME2A and GOME2B instruments

During the first inspection of the three datasets by both the GDP4.9 algorithm and the ACSAF SO_2 validation teams, it was found that the solar irradiance spectrum for GOME2A and GOME2B shows a sudden wavelength shift from one orbit to the other, inducing a strong negative bias in the resulting SCDs. This unstable behavior in the wavelength calibration is caused by the spectral light source lamp in the wavelength region 312-330 nm. An alternative Solar Fraunhofer line spectral calibration algorithm is currently under implementation and will be integrated in the GOME2 L1 Product Processing Function (planned for Q2/2021).

While during year 2018 these shifts appeared to be sporadic in nature affecting one orbit every so many others, after the beginning of 2019 these show to be omnipresent. These "jumps" are demonstrated in Figure 1, where the GOME2/MetopA daily sequence over an Equatorial region, which is free of SO_2 sources and should have shown near-zero SCDs, is shown in the upper panel and GOME2/MetopB in the lower panel for days in 2018 and 2019. These discontinuities, long reported to EUMETSAT, result in non-continuous orbital SO_2 VCDs, as shown for an entire day in May 2018 for GOME2B in Figure 2. The GOME2/MetopB SO_2 VCD at 15km for the 1st of May 2018 is used as demonstration of the effect of the solar irradiance spectrum wavelength shift.

EUMETSAT
AC SAF

REFERENCE: **SAF/AC/AUTH/VR/SO2**
ISSUE: 11/2020
DATE: 30/11/2010
PAGES: Page **13** of **62**
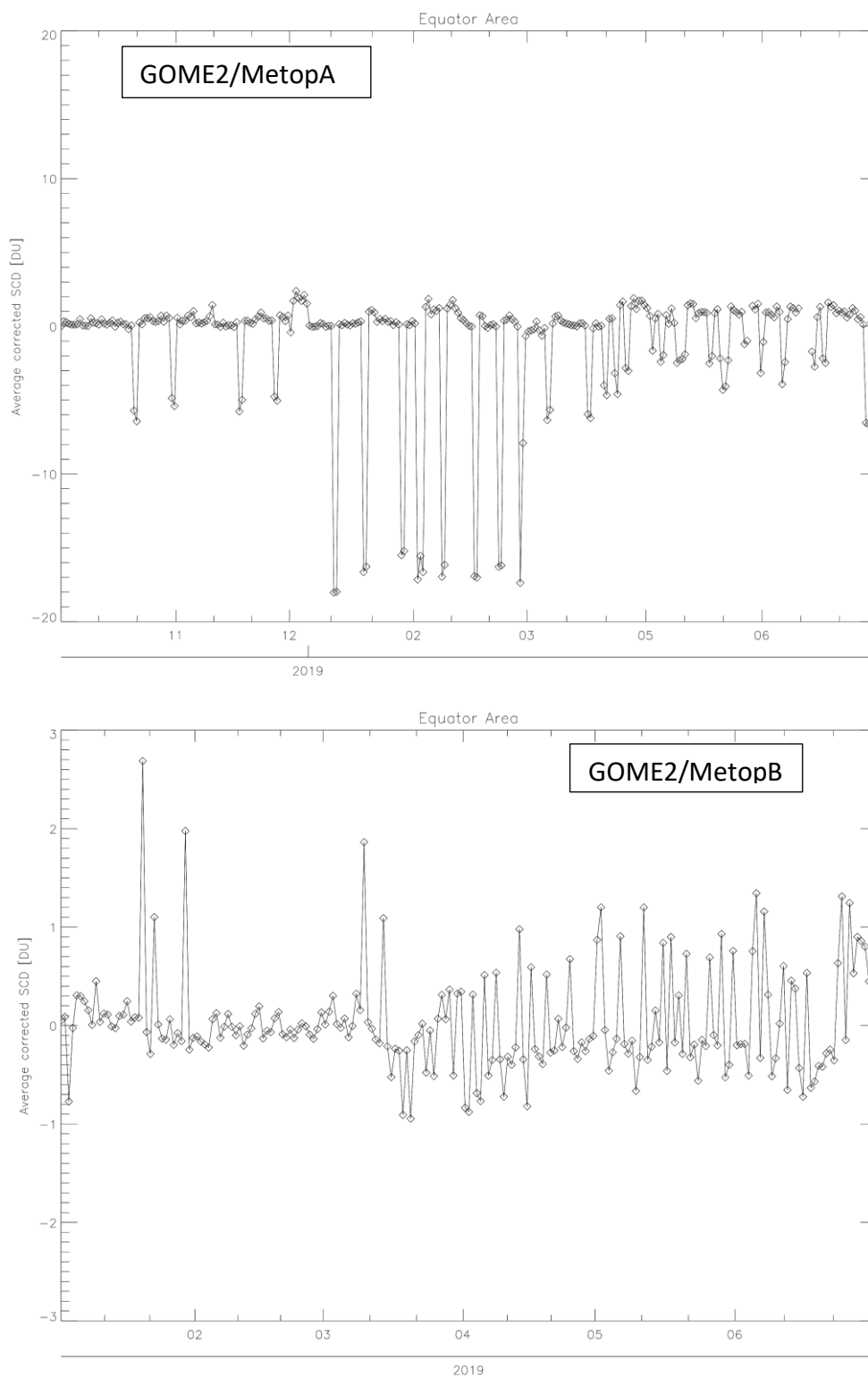
Figure 1. Slant Column Densities over an Equatorial region for GOME2/MetopA [upper] and GOME2/MetopB [lower] for months in 2018 and 2019.
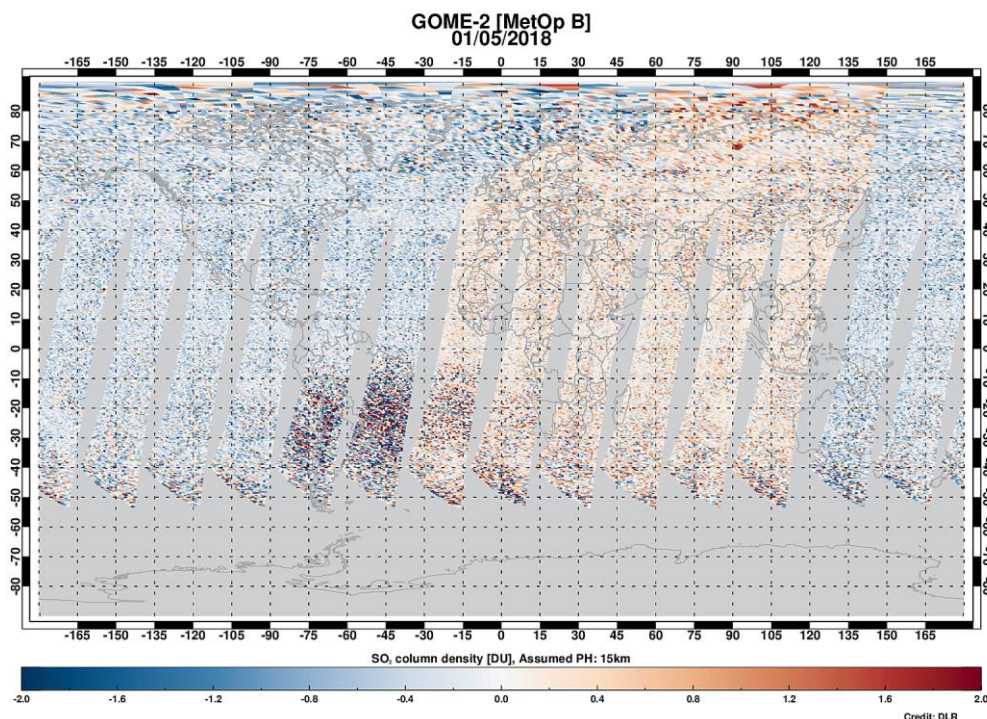
Figure 2. GOME2/MetopB SO_2 VCD at 15km for the 1st of May 2018 used as demonstration of the effect of the solar irradiance spectrum wavelength shift.

For the purposes of this validation exercise, we examined this effect on the monthly mean SCDs reported by GOME2A, GOME2B and GOME2C, filtered and gridded as discussed in Section 2.1, for the month of May 2019 [upper, middle and lower panel respectively in Figure 3.] The daily "jumps" are of course smoothed out in this representation but the overall differences in the levels of the SCSs, plotted within ±2 D.U., with the minima and maxima of the ranges also given, can be observed. In Figure 4 the time series, during the month of May 2019, of the SCDs over an Equatorial box are shown both on a pixel basis [upper] and as a daily spatially average [lower], further testifying to the relative differences between the three instruments.

As a result of the above analysis, it was decided to avoid direct comparisons between the three sister instruments, as means to validate the GOME2/MetopC instrument.

GOME2/MetopA

GOME2A | SO2 Slant Column Number Density
May 2019 | 0.25x0.25

SO2 SCD [D.U.]

-2.0   -0.8   0.4   1.6   2.8   4.0
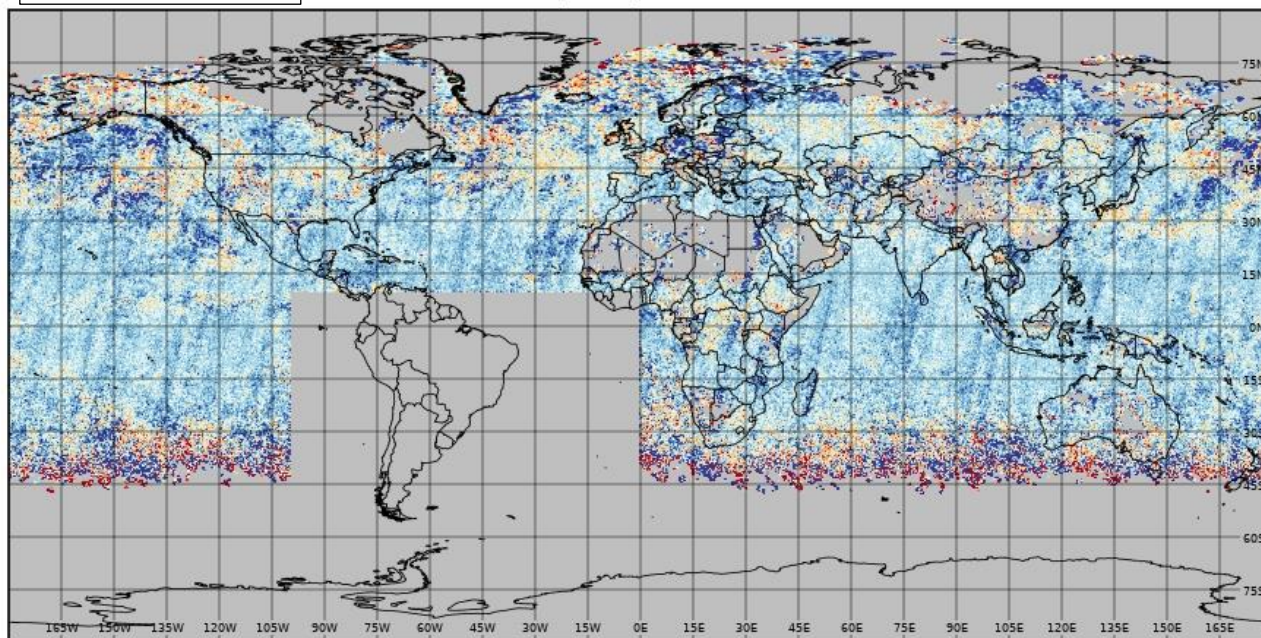
Data Min = -18.7, Max = 19.2, Mean = 0.2

GOME2/MetopB

GOME2B | SO2 Slant Column Number Density
May 2019 | 0.25x0.25

SO2 SCD [D.U.]

-2.0 -1.6 -1.2 -0.8 -0.4 0.0 0.4 0.8 1.2 1.6 2.0
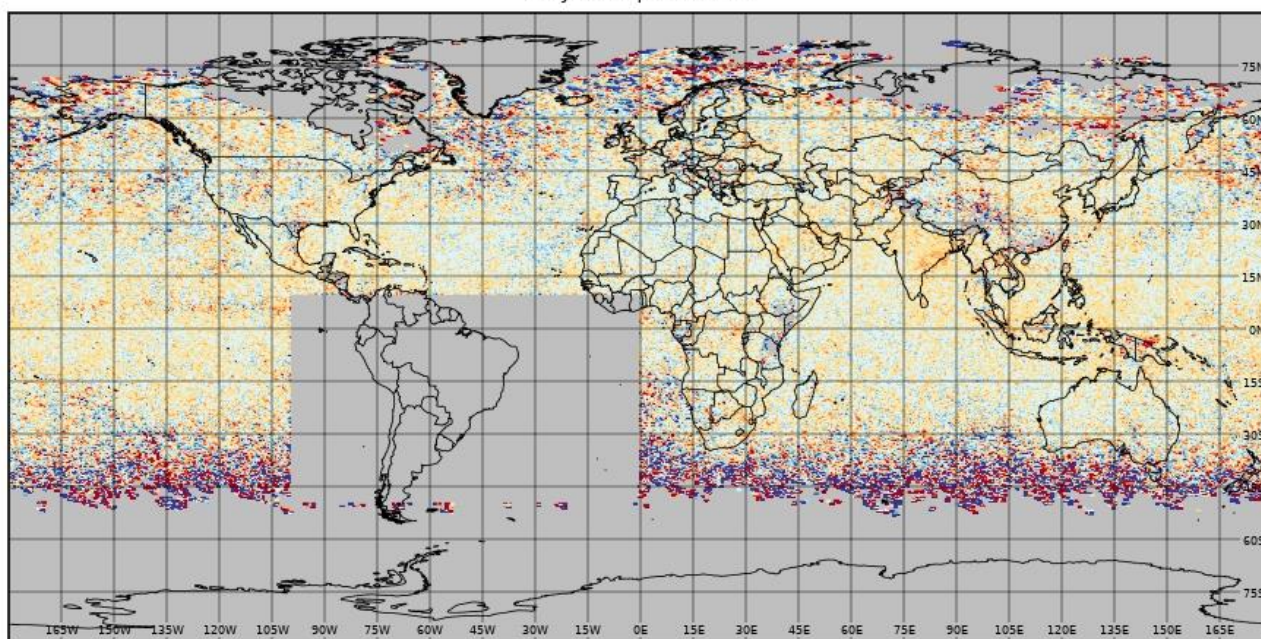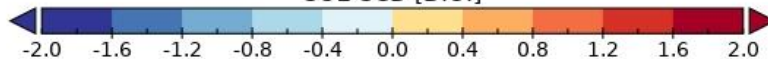
Data Min = -18.7, Max = 15.7, Mean = 0.0
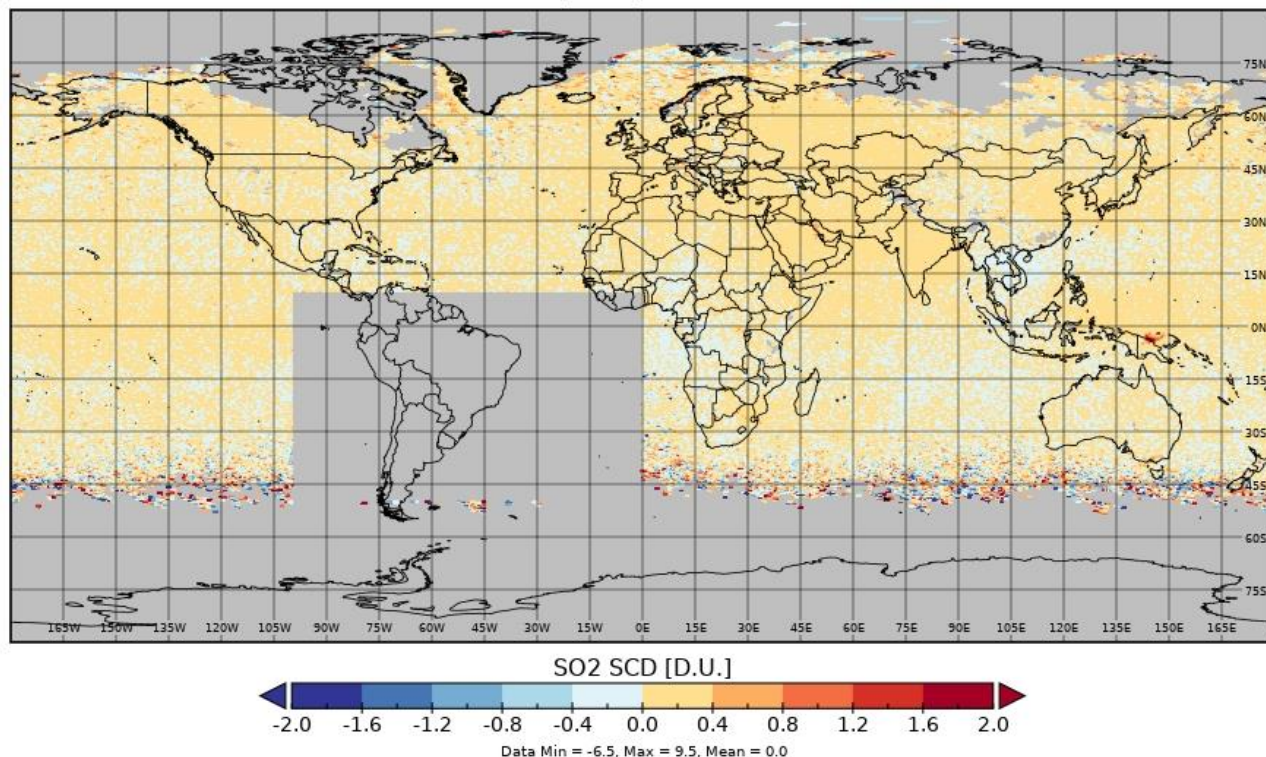
Figure 3. SO$_2$ Slant Column Density for May 2019 filtered and on a 0.25x0.25° grid for the GOME2/MetopA [upper], GOME2/MetopB [middle] and GOME2/MetopC [lower panel] observations on the same colour scale.

SCD over an Equatorial Box | May 2019
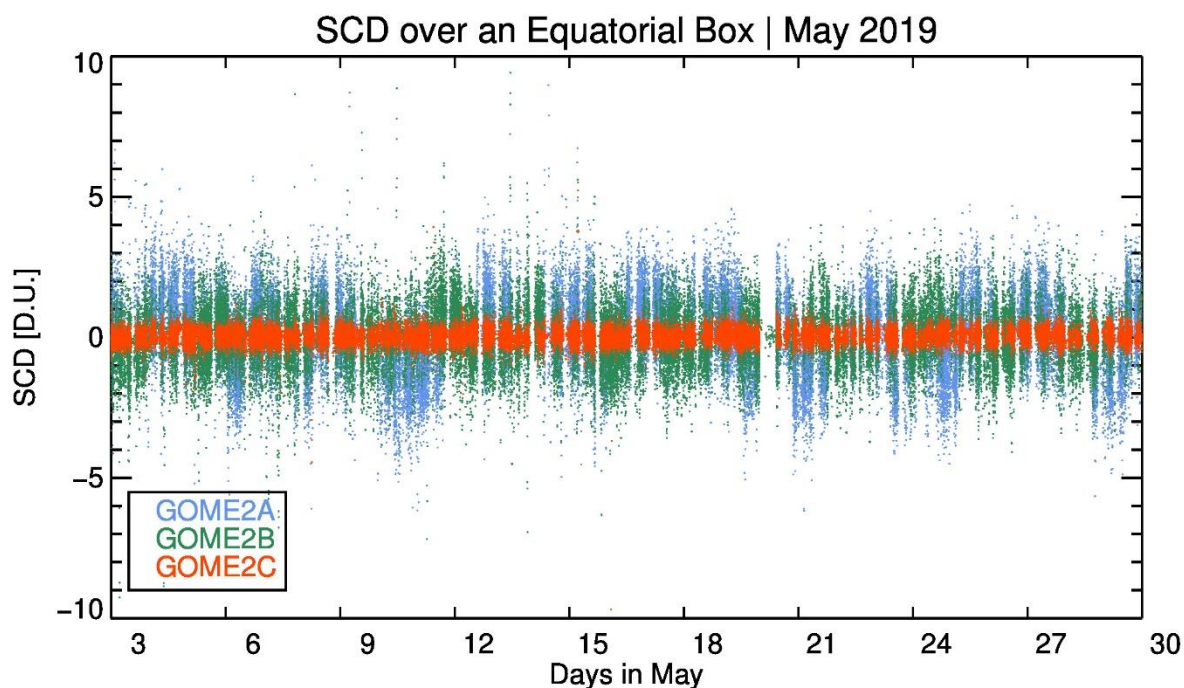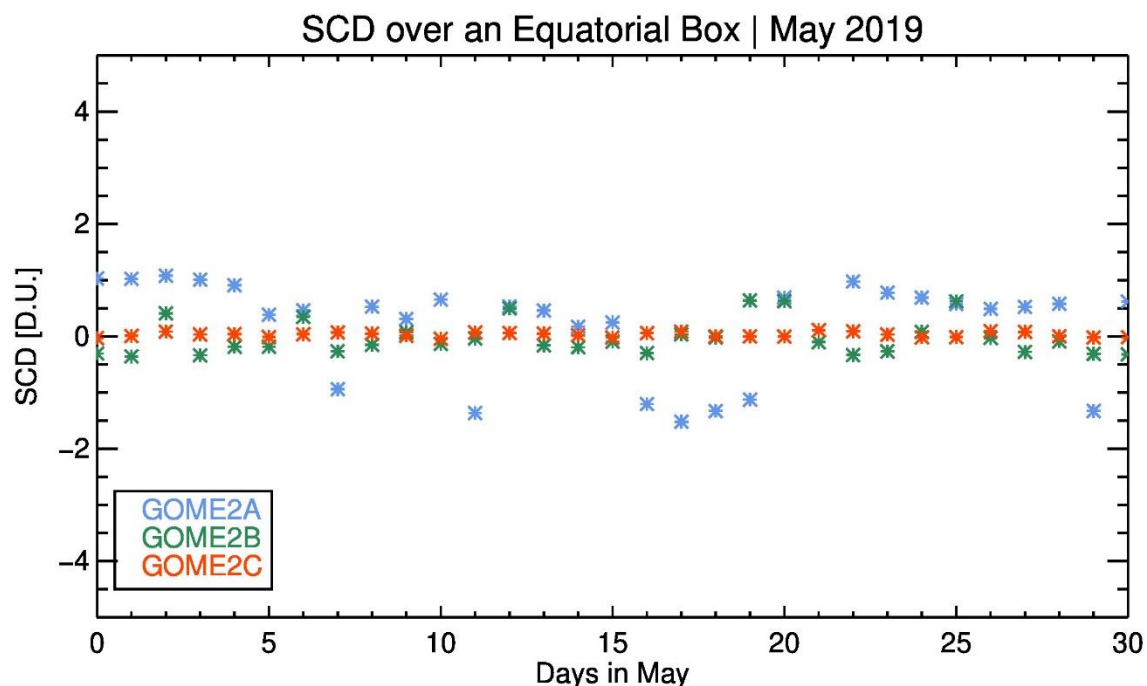
Figure 4. Daily SO$_2$ SCDs per pixel [upper] and area averaged [lower] for May 2019, filtered and on a 0.25x0.25° grid, for the latitudes between 0 and 15°N and longitudes between -120 and -105°E, for GOME2A [blue], GOME2B [green] and GOME2C [red].

1.3   Total SO$_2$ GOME2/Metop Product requirements

In the following we reproduce the table that pertains to the total sulphur dioxide GOME2/Metop products where the accuracy requirements are given as 100% [threshold], 50% when the SZA <70° [target] and 30% as the optimal accuracy.

Table 2.The relevant table from the Product Requirements Document [PRD].

Total SO$_2$	
NRT: O3M-54.1, O3M-55.1, O3M-374 Offline: O3M-09.1, O3M-56.1, O3M-375	MAG-N-SO2, MBG-N-SO2, MCG-N-SO2 MAG-O-SO2, MBG-O-SO2, MCG-O-SO2
Type	Product
Applications and users	Volcanic emissions, SACS, VAACs, TEMIS, research institutes, anthropogenic emission monitoring, MACC/CAMS
Characteristics and methods	DOAS slant column fitting + AMF conversion
Generation frequency	NRT: PDU dissemination frequency, every 3 minutes on daylight side of orbit Offline: Metop orbit repeat cycle
Input satellite data	Metop-A/B/C: GOME-2

Algorithm version	Metop-A/B: GDP 4.8 Metop-C: GDP 4.9	
Dissemination		
Type	Format	Means
NRT	BUFR, HDF5	EUMETCast, WMO GTS
Offline	HDF5	FTP
Accuracy		
Threshold	**Target**	**Optimal**
100 %	**50 % (SZA < 70˚)**	**30 %**
Verification method	**Comparison with ground-based measurements** **Satellite-to-satellite comparison**	
Coverage, resolution and timeliness		
Spatial coverage	Spatial resolution	Timeliness
Global	GOME-2/Metop-A: nominal pixel size 80 x 40 km^2 (before 15 July 2013) nominal pixel size 40 x 40 km^2 (after 15 July 2013) GOME-2/Metop-B/C: nominal pixel size 80 x 40 km^2	NRT ≤ 3 hours Offline ≤ 2 weeks
Comments		
A specific volcanic SO$_2$ detection flag to identify enhanced GOME-2 SO$_2$ levels and to separate these measurements from GOME-2 pixels with high noise levels is required for use of GOME-2 SO$_2$ columns in CAMS. This volcanic SO$_2$ flag is included in the NRT and Offline GOME-2 Total SO$_2$ products. ~~A specific volcanic SO2 detection flag to identify enhanced GOME-2 SO2 levels and to separate these measurements from GOME-2 pixels with high noise levels is required for use of GOME-2 SO2 columns in MACC and CAMS. This volcanic SO2 flag will be included in the NRT and Offline GOME-2 Total SO2 products.~~		

2   DATA SOURCES

In the following section we briefly give the relevant information on the different space-based datasets used in this report, including the main related documents and open source links.

2.1   GOME2 OFFL L2 orbital files

The validation dataset for the GOME2/MetopC observations was delivered from DLR via ftp to include all days from February 1st to July 31st 2019, based on the offline GDP4.9 algorithm discussed in Section 1.1. The GOME2/MetopA and GOME2/MetopB offline level-2 orbital files are routinely downloaded into the LAP/AUTH validation chain, as part of the operational ACSAF validation services.

From the group 'DETAILED_RESULTS/SO2/', the 'VCDCorrected' array was extracted, which contains the anthropogenic and volcanic SO_2 load used further on, as well as the 'ESCCorrected', the Slant Column Density, and the 'VCDCorrected_Error', the associated error to the VCD columns.

All three GOME2 instruments, for the case of the anthropogenic VCD, where filtered as recommended using:

> Cloud fraction ≤ 0.20 & SZA ≤ 75 & forward scans only & so2_flag = 0

The orbital files where transformed into HARP-compliant daily files using in-house code, for direct manipulation with the standard HARP commands.

2.2   S5P/TROPOMI orbital files

The S5P/TROPOMI offline orbital files between February and July 2019 were downloaded from the S5P pre-operations hub, https://s5phub.copernicus.eu/dhus/#/home, data version 01.01.07. The relevant ATBD can be found here, http://www.tropomi.eu/document/atbd-sulphur-dioxide and the PUM here, http://www.tropomi.eu/document/product-user-manual-sulphur-dioxide-0. The TROPOMI SO_2 data are routinely validated via the S5P Mission Performance Center Validation Facility, http://mpc-vdaf.tropomi.eu/, and the more recent Quarterly Validation Report of the Sentinel-5 Precursor Operational Data Products #08: April 2018 – August 2020, can be accessed here: http://mpc-vdaf.tropomi.eu/ProjectDir/reports/pdf/S5P-MPC-IASB-ROCVR-08.01.01-20200921_FINAL.pdf .

From the group '/PRODUCT/' the fields 'sulfurdioxide_total_vertical_column' and 'sulfurdioxide_slant_column_corrected' were extracted.

For the case of the S5P/TROPOMI data, these were filtered, as recommended, using the following clauses:

> Cloud fraction ≤ 0.20 | SZA ≤ 75 | QA > 50 | AMF ≥ 0.2 | Ice flag ≤ 0.5 | rows ≥ 22 and ≤ 429

The S5P orbital files where the transformed into HARP-compliant daily files using in-house code, for direct manipulation with the standard HARP commands.

2.3 OMI/Aura L3 daily files

The daily level-3 OMI/Aura SO2 dataset was downloaded using the NASA EarthData open source repository, https://acdisc.gesdisc.eosdis.nasa.gov/data/Aura_OMI_Level3/OMSO2e.003/2019/. In the OMI/Aura Sulfur Dioxide (SO$_2$) Total Column Daily L3 1 day Best Pixel in 0.25 degree x 0.25 degree V3 (OMSO2e) each grid contains only one observation of Total Column Density of SO$_2$ in the Planetary Boundary Layer (PBL), based on an improved Principal Component Analysis (PCA) Algorithm. This single observation is the "best pixel", selected from all "good" L2 pixels of OMSO2 that overlap this grid. The algorithm is described in Li et al., 2020a, and the dataset is referenced as Li et al., 2020b. The pertinent details of how the OMI level-2 orbital files have been transformed into a level-3 daily dataset can be found here: https://acdisc.gesdisc.eosdis.nasa.gov/data/Aura_OMI_Level3/OMSO2e.003/doc/README.OMSO 2e_2020-10-16.txt. The main filters used are enumerated here, for easy comparison to the ones used for the rest of the space-born datasets presented in this report:

These filters are summarized here in sequence, where level-2 observations that comply with the following list where excluded:

> Raised solar eclipse possibility flag.
>
> Row anomaly flag.
>
> CTP< 3 and CTP>58.
>
> Cloud radiance fraction > 0.2 or < 0
>
> SZA > 70
>
> AMF < 0.3
>
> South Atlantic Anomaly flag

3   COMPARISON AND VALIDATION ANALYSIS

3.1   Comparison of Slant Column Densities

Further to the discussion in Section 1.2, before comparing VCDs, we show further examples of the relative SCD levels between GOME2C and GOME2B & S5P/TROPOMI. In Figure 5, the bi-monthly, cloud-filtered, and averaged SO_2 slant column density maps for April and May 2019 are given for GOME2B, upper, GOME2C, middle, and TROPOMI, lower panels.
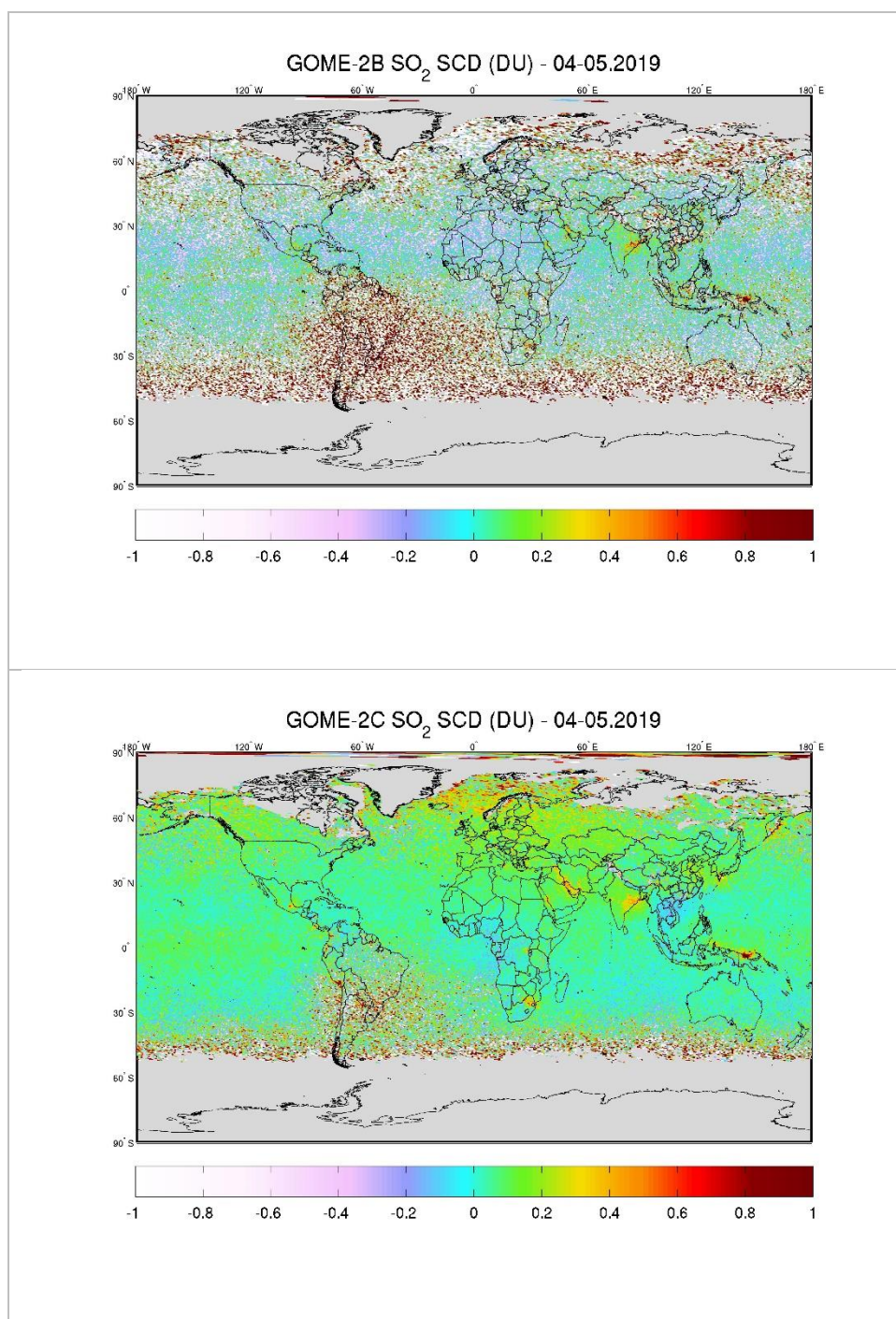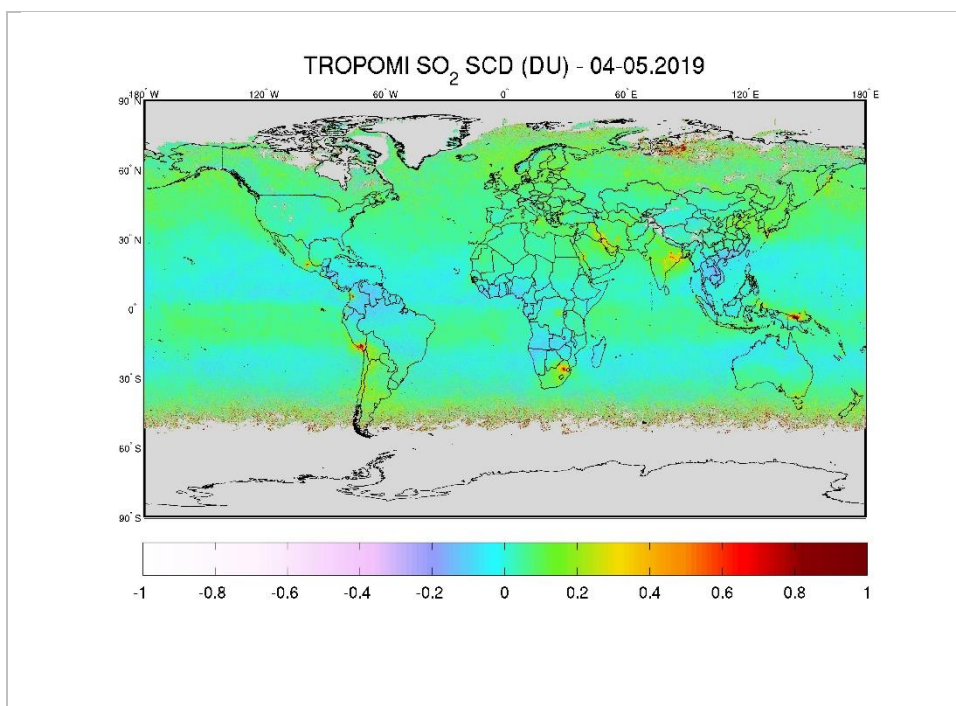
Figure 5. Bi-monthly averaged SO$_2$ slant columns maps for April and May 2019 for GOME2B [upper], GOME2C [middle] and TROPOMI [lower] observations.

From Figure 5, the following assertions may be made:

- The noise level is much reduced in the new GOME2C data set compared to the GOME2B one and therefore several SO$_2$ spots appear more clearly. This is a great advantage of using the 312-326 nm range compared to 315-326 nm.
- The GOME2C results are much less sensitive to the South Atlantic Anomaly. However, this region is entirely masked when the recommendation to use the so2_flag = 0 is met.
- Generally, the bias at high latitudes are much less present with GOME2C than GOME2B. The GOME2C results seems to be slightly biased high overall by 0.1-0.2 DU and this could be potentially be solved by an improved background correction.
- The agreement between GOME2C and TROPOMI is fairly good overall.

3.2   Anthropogenic SO₂ Pollution Vertical Column Density

3.2.1   Comparisons with OMI/Aura

In Figure 6 the GOME2C pollution VCD is compared to the equivalent one reported by the OMI/Aura instrument on a 0.25x0.25° regular grid. The ranges of the reported values vary significantly, hence different colour scales were chosen for the depiction, with the GOME2C maps rising to 2 D.U but the OMI maps to 1 D.U. The month of March [upper row] and May [lower row] are shown here to show the possible seasonality in the relative levels reported, as the sources shown in blue in the left column are continuously emitting lignite power plants and outgassing volcanoes, namely Mt. Etna and Stromboli, in Italy. The GOME2C monthly mean map is shown to be noisy and post-processing of the monthly fields would be required for a direct comparison [i.e. difference] to other satellite fields.

Figure 6. Left. Map of the SO₂ pollution VCD [D.U.] in Eastern Europe, including multiple sources as blue labels, for March 2019 of GOME2/MetopC [upper] and May 2019 of GOME2/MetopC [lower] observations gridded onto a regular 0.25x0.25° grid. Right. Same for the OMI/Aura SO₂ pollution VCD [D.U.]. Note that the colour scales are different.

Figure 7. Left. Map of the SO_2 pollution VCD [D.U.] in South Africa including multiple sources as blue labels, for March 2019 of GOME2/MetopC [upper] and May 2019 of GOME2/MetopC [lower] observations gridded onto a regular 0.25x0.25° grid. Right. Same for the OMI/Aura SO_2 pollution VCD [D.U.]. Note that the colour scales are different.

As for Figure 6, Figure 7 shows the GOME2C monthly mean SO_2 pollution VCD over the Southern African states compared to the observations by OMI/Aura. The noise levels over the sea regions in this case render a one-to-one comparison impossible without further filtering of the original dataset. The increase in the noise level below 30°S is clear, possibly due to the high SZA values in the Southern Hemisphere during these months. **This could be an indication that the recommendation of filtering with SZA<75° should be reconsidered to a stricter range of acceptable values.**
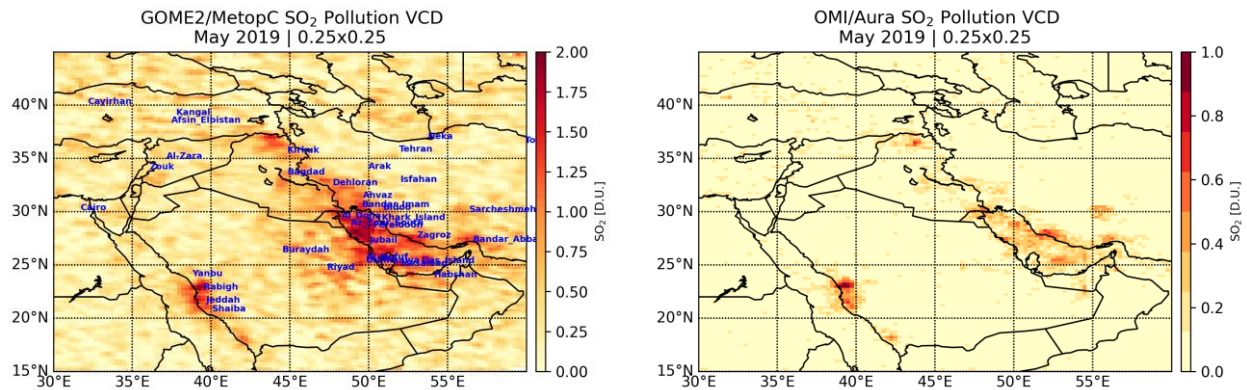
Figure 8.Left. Map of the SO$_2$ pollution VCD [D.U.] in the Middle East Africa including multiple sources as blue labels, for March 2019 of GOME2/MetopC [upper] and May 2019 of GOME2/MetopC [lower] observations gridded onto a regular 0.25x0.25° grid. Right. Same for the OMI/Aura SO$_2$ pollution VCD [D.U.]. Note that the colour scales are different.

Even though the actual VCD loads between GOME2C and OMI differ by a substantial amount, for the Middle Eastern domain [Figure 8], scatter plots of the monthly mean loads were calculated over the highest anthropogenic emitting locations on a global scale reported by Violetov et al., 2020, and enumerated in Table 5 to Table 7, of the Appendix. In the left column of Figure 9, the monthly mean VCDs reported by GOME2C [x-axis] and OMI [y-axis] are compared for the Middle East and namely, for 13 Oil and Gas point source locations [first row], 6 Power Plant locations [second row] and 1 Smelter location [bottom row.] Even though the relative loads between the two instruments are quite different, with GOME2C over-estimating [or OMI under-estimating] by nearly an order of magnitude, the very promising correlation coefficients [0.67, 0.67 and 0.55 respectively for the three types of sources] point to the fact that the two instruments capture the relative magnitudes correctly, albeit not the actual SO$_2$ load levels.

It has long been assumed that to directly compare different satellite VCDs, extracted using a DOAS or DOAS-type methodology, the Slant Column Densities should be compared, divided by a common AMF value, so as to exclude differences in the AMF calculations which translate into significant differences in the resulting VCDs. In the right column of Figure 9, these calculated quantities, namely the SCDs divided by a common AMF of 0.4, are compared. The slopes of the comparisons improve by more than twice, while the y-intercept and correlations, more or less do no alter. This fact further testifies to the fact that the sources are identified well by GOME2C observations even though the absolute magnitudes do not precisely coincide with the OMI/Aura observations.

Table 3. Mean value, standard deviation and correlation coefficient for the monthly mean ~~Statistics for the~~ comparisons of the different point sources of anthropogenic SO$_2$ over the Middle East, referring to Figure 9, between February and July 2019.

		GOME2C Mean [D.U.]	Std [D.U.]	OM/Aura Mean [D.U.]	Std [D.U.]	R^2
Power Plant	SO$_2$ SCD/0.4	0.6737	0.3097	0.4006	0.3991	0.5467
Smelter		0.9558	0.4181	0.5163	0.4462	0.5478
Oil and Gas		0.5723	0.3473	0.3807	0.4063	0.6690
Power Plant	SO$_2$ VCD	0.8294	0.4287	0.2566	0.2520	0.6679
Smelter		0.7863	0.3428	0.2217	0.1903	0.5494

Oil and Gas			0.7995	0.4925	0.2338	0.2700	0.6666

Figure 9. Left. Comparisons of the GOME2C monthly mean SO₂ pollution VCDs for the entire period of February to July 2019 over the Middle Eastern region enclosed by Figure 8 to the OMI/Aura VCDs for 13 Oil and Gas sources [upper], 6 Power Plants [middle] and 1 Smelter [lower.] Right. Same for the SCD/0.4 [D.U.] comparisons.

3.2.2   Comparisons with S5P/TROPOMI

We first compare the relative SO$_2$ VCD levels reported by GOME2C [left columns] and TROPOMI [right columns] as map representations of the monthly mean values for different locations around the world with known anthropogenic emissions sources. In Figure 10, the SO$_2$ VCDs for the month of March 2019 [upper] and May 2019 [lower] are given for the Eastern China domain, whereas in Figure 11 the same is given for the Middle East and in Figure 12 for India. The names of the known emission sources are given in blue. The low SO$_2$ values over Eastern China revealed by both sensors are well in line with the current assessment that the pollution is much reduced in those regions due to the stringent environmental legislation that has been applied during the last few years over China. Over Middle East and India the sources are more pronounced, with the smaller pixel size of TROPOMI pointing directly at the specific locations. Overall the two sensors report similar magnitude VCDs which allow us to proceed to a more detailed numerical comparison at different spatiotemporal scales.

Figure 10. Left. Map of the SO$_2$ pollution VCD [D.U.] in Eastern China including multiple sources as blue labels, for March 2019 of GOME2/MetopC [upper] and May 2019 of GOME2/MetopC [lower] observations gridded onto a regular 0.25x0.25° grid. Right. Same for the S5P/TROPOMI SO$_2$ pollution VCD [D.U.].
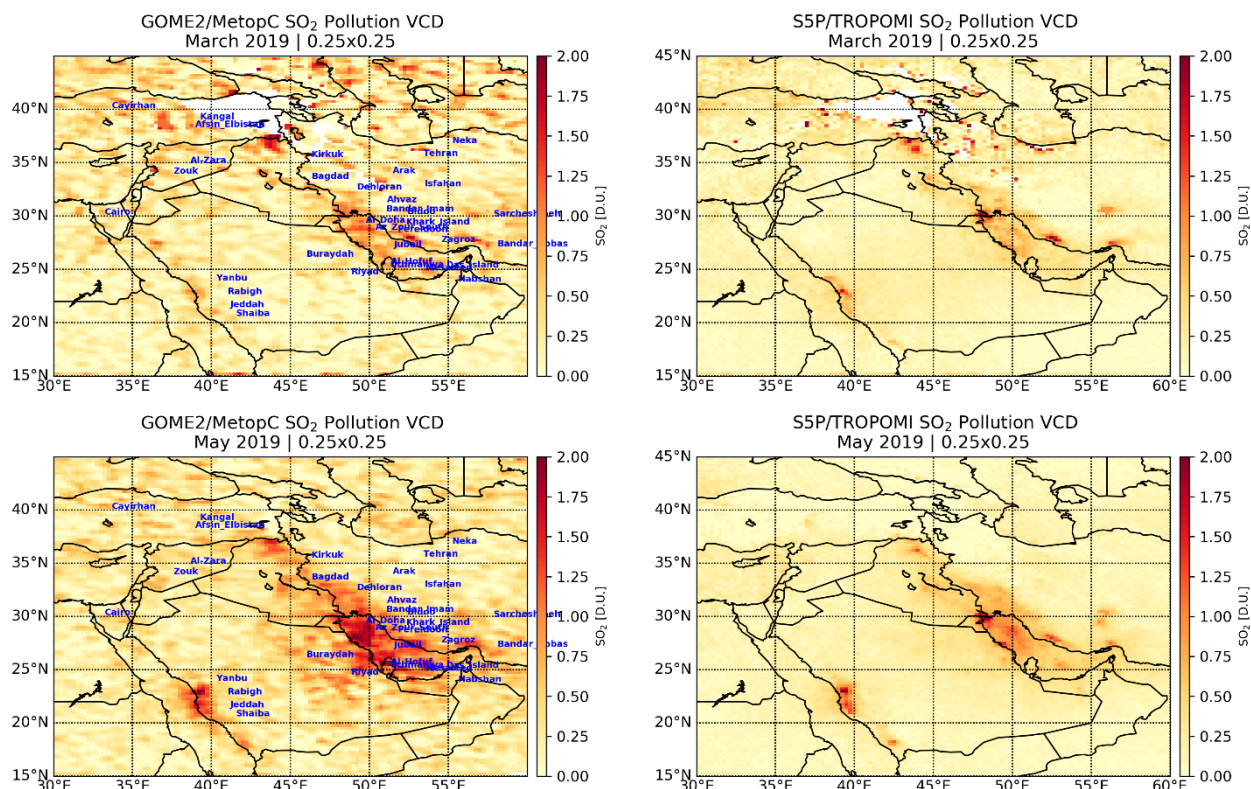
Figure 11 Left. Map of the SO₂ pollution VCD [D.U.] in the Middle East including multiple sources as blue labels, for March 2019 of GOME2/MetopC [upper] and May 2019 of GOME2/MetopC [lower] observations gridded onto a regular 0.25x0.25° grid. Right. Same for the S5P/TROPOMI SO₂ pollution VCD [D.U.].
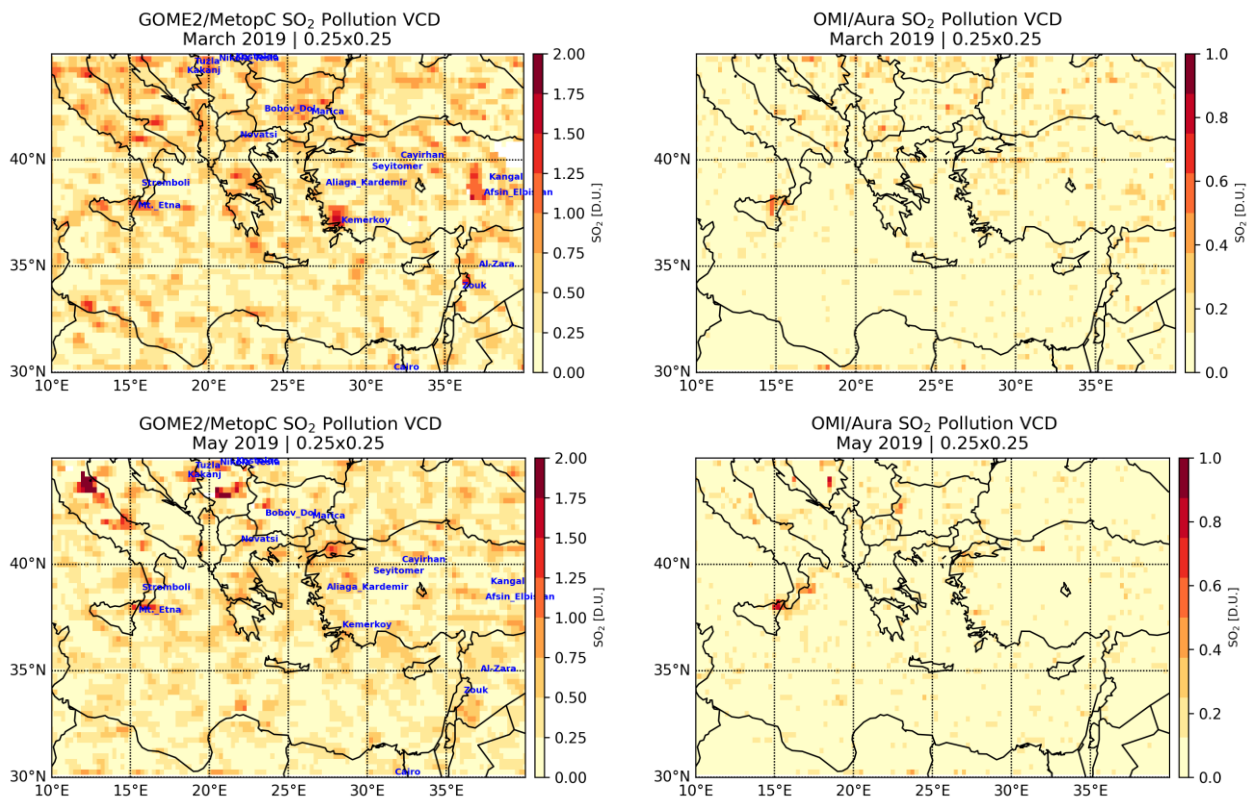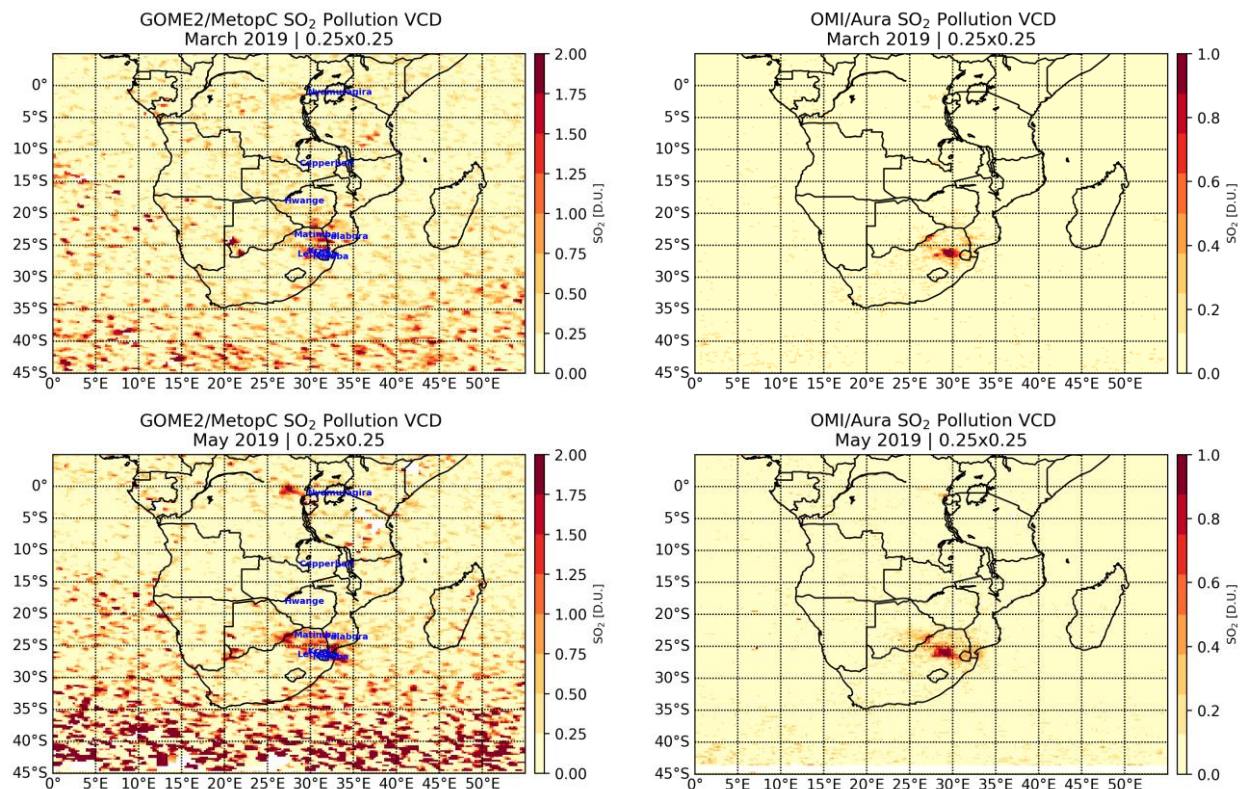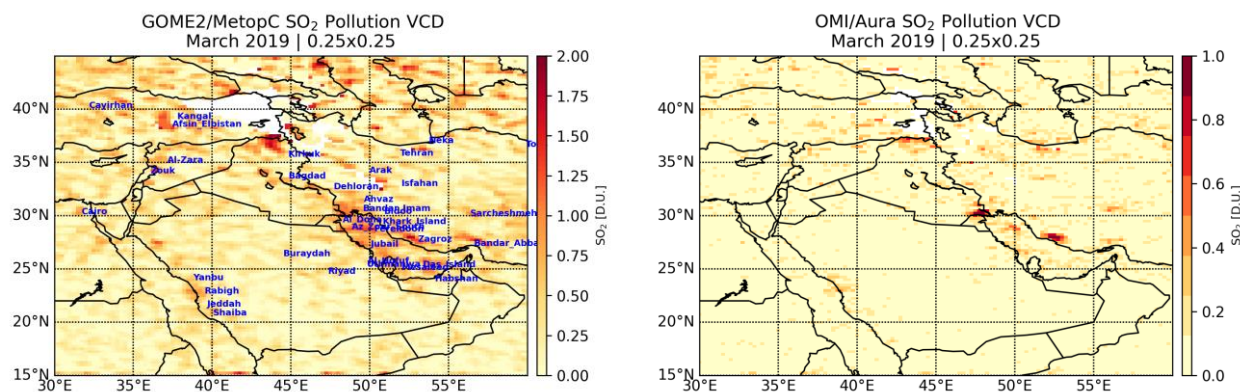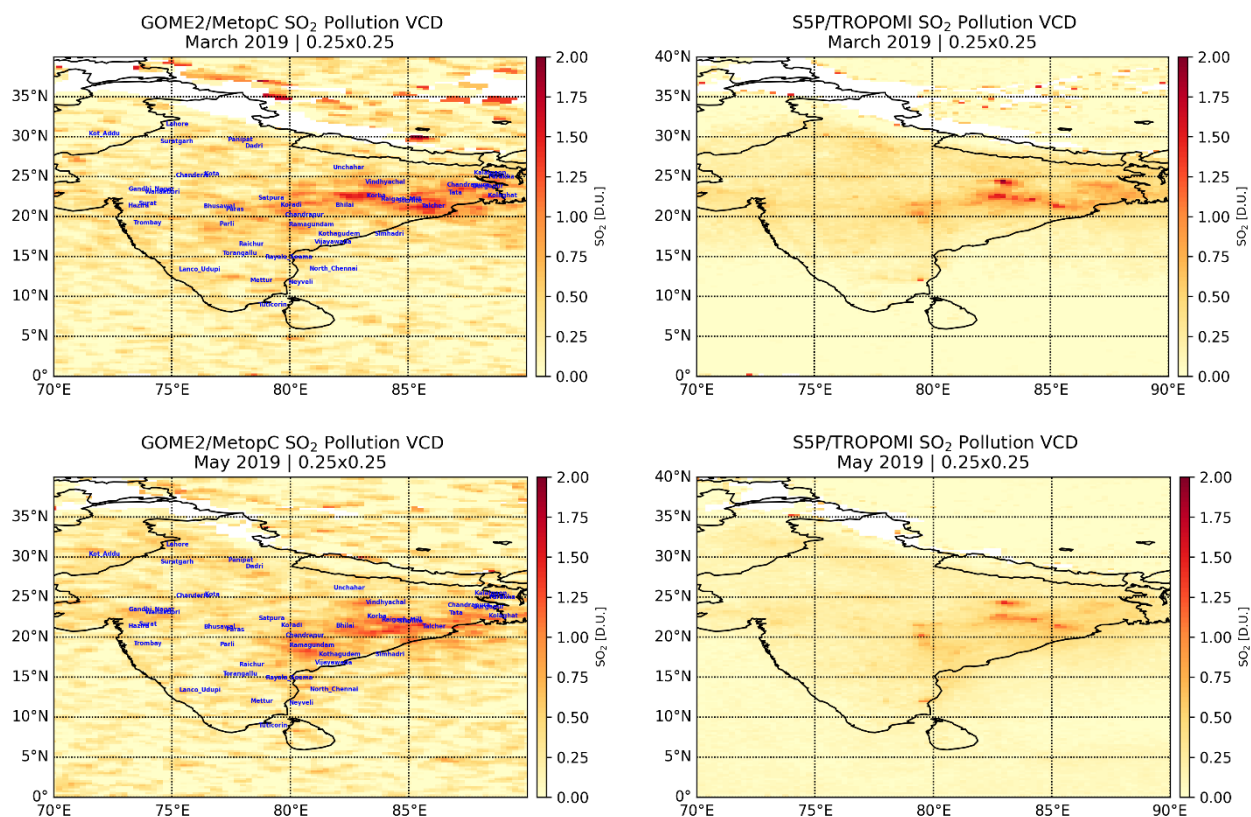
Figure 12. Left. Map of the SO_2 pollution VCD [D.U.] over India including multiple sources as blue labels, for March 2019 of GOME2/MetopC [upper] and May 2019 of GOME2/MetopC [lower] observations gridded onto a regular 0.25x0.25° grid. Right. Same for the S5P/TROPOMI SO_2 pollution VCD [D.U.].

3.2.2.1 Comparing per type of source on a daily temporal scale

In order to assess the usability of the GOME2C anthropogenic pollution VCD, as reported in the orbital files, in the following we show scatter plot comparisons between GOME2C and TROPOMI levels, from the calculated 0.25x0.25° grids, based on the highest anthropogenic emitting locations on a global scale reported by Violetov et al., 2020, and enumerated in Table 5 to Table 7, of the Appendix. The daily mean SO_2 level, smoothed by the two surrounding cells in all directions, show that, for 22 locations of Oil and Gas sources Figure 13 [upper] the daily mean VCDs compare relatively well, with GOME2C over-estimating the TROPOMI VCDs with values rising to 3 D.U. Similarly for the 39 Power Plant locations (Figure 13, middle) even though in this case the range of values is similar between sensors with GOME2C overestimating. In Figure 13, lower, the comparisons over 7 Smelter locations is the least promising, possibly due to the, in general, lower VCDs observed above such sources.
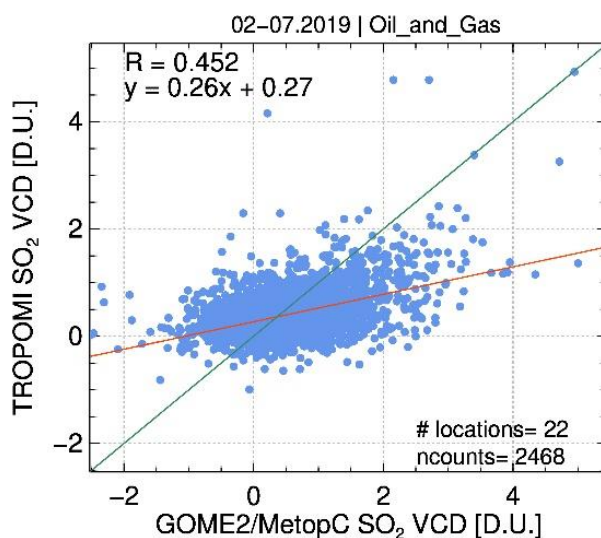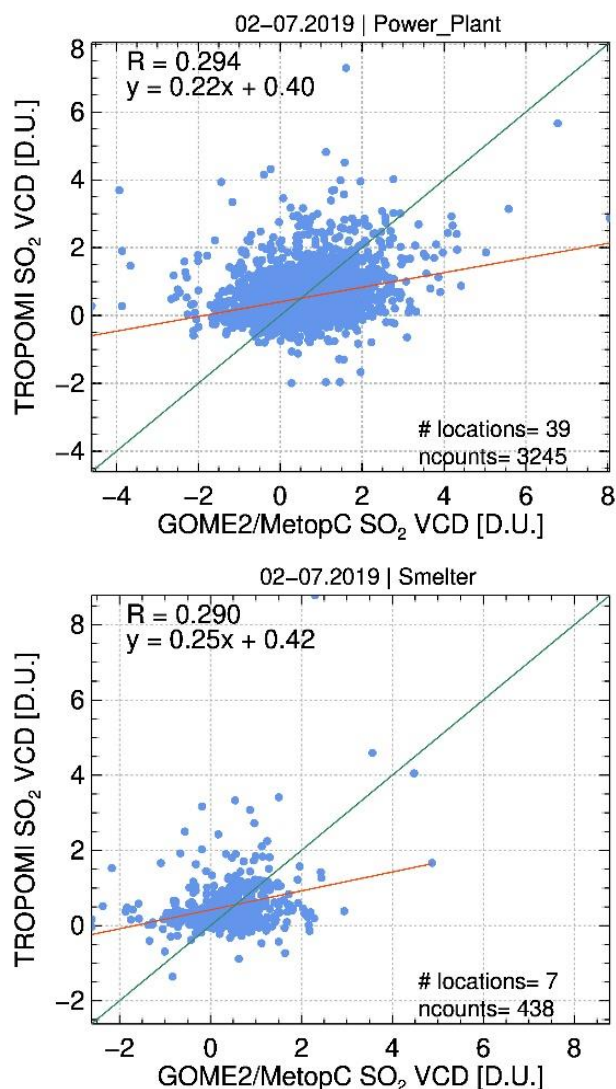
Figure 13. Daily mean SO$_2$ pollution VCDs for the time period February to July 2019 as reported by GOME2C [x-axis] are compared to theS5P/TROPOMI VCDs for all Oil and Gas [upper], Power Plant [middle] and Smelter sources [lower] given in Table 5 to Table 7.

The above comparisons where repeated using the Slant Column Density reported by each instrument divided by and AMF = 0.4, and are shown in Figure 14. Overall the ranges of levels reported do not change, nor does the comparison improved in a marked manner.
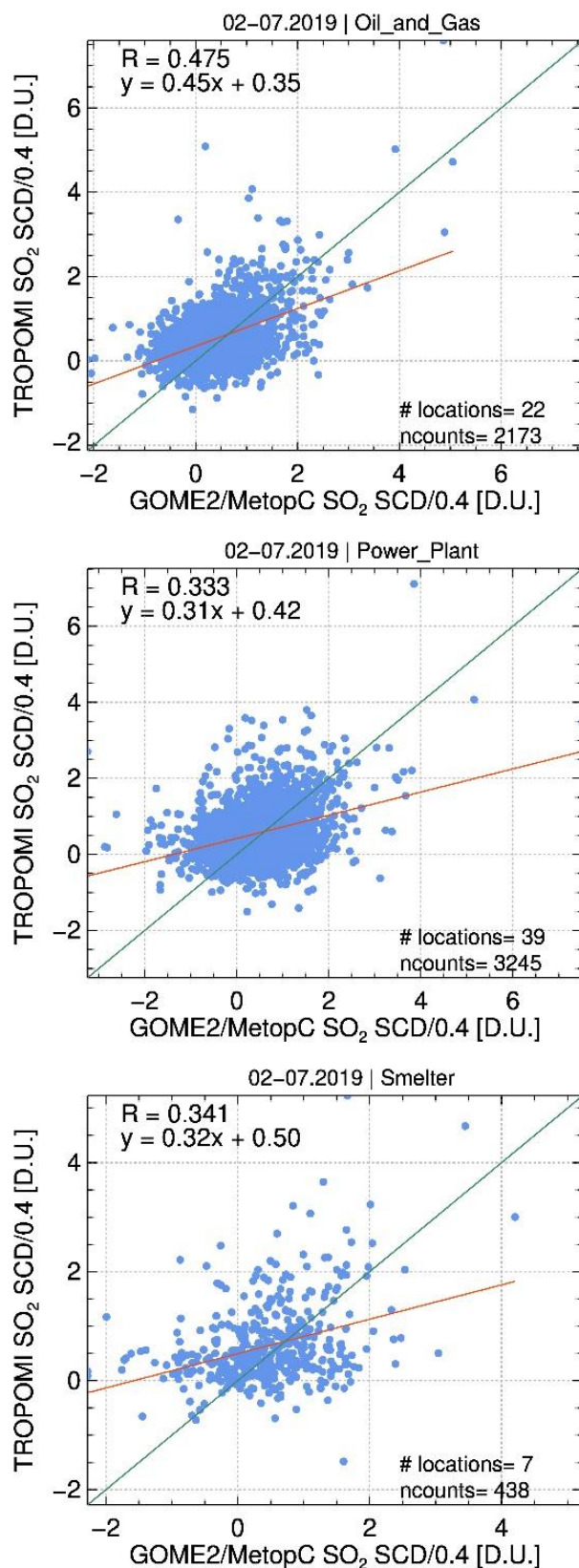
Figure 14. Daily mean SO_2 pollution SCDs, divided by AMF = 0.4, for the time period February to July 2019 as reported by GOME2C [x-axis] are compared to the S5P/TROPOMI VCDs for all Oil and Gas [upper], Power Plant [middle] and Smelter sources [lower] given in Table 5 to Table 7.

3.2.2.2   Comparing per region on a daily temporal scale

In this section we examine the capabilities of the GOME2C anthropogenic SO₂ product in assessing regional SO₂ levels on a daily temporal scale, and not point sources, as shown in Section 3.2.2.1.

We have also compared time series of GOME2C and TROPOMI post-calculated VCDs from the reported SCDs assuming a fixed AMF of 0.4 for consistency over entire regions with known anthropogenic hotspots, namely: India, [20,25]°N and [80,87]°E ; Middle East, [23,32]°N and [45,60]°E ; South Africa, [-28,-25]°N and [27,32]°E; China, [35,40]°N and [110,120]°E and Peru, [-18,-14]°N and [-75,-70]°E . In Figure 15, the timeseries comparisons over the region of Peru is shown, where the two instruments show a reasonable agreement on the daily temporal scale. In Figure 16, a scatter plot of all regions examined is shown.
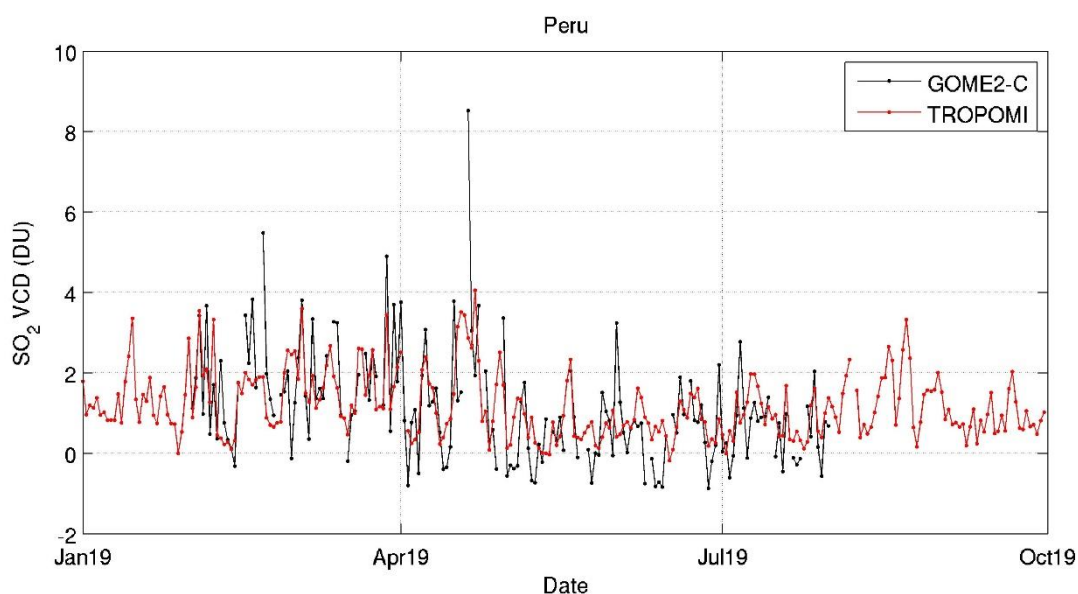
Figure 15. Timeseries of the daily mean VCDs, extracted by SCD/0.4, for GOME2C [black] and TROPOMI [red] between January and September 2019.
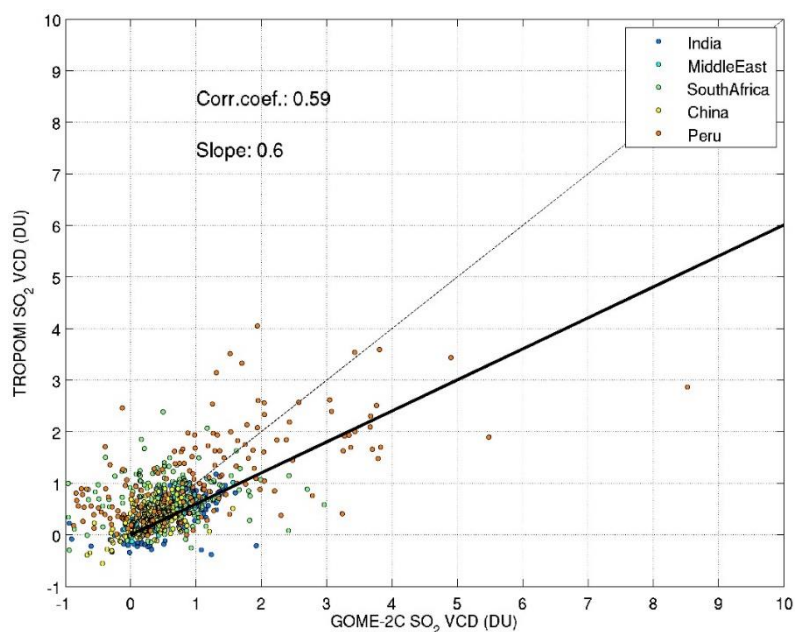
Figure 16. Scatter plot of the daily mean VCDs, extracted by SCD/0.4, for GOME2C [xaxisblack] and TROPOMI [yaxisred] between January and July 2019 for all regions examined in this subsection, given in different colours as per the legend.

3.2.2.3   Comparing per type of source on a monthly mean time scale

Even though on a daily basis the comparisons over known and strong hot-spots of anthropogenic SO_2 are not providing higher correlations than 0.475, things improve significantly on a monthly mean time scale as shown in Figure 17 and in Figure 18. In Figure 17, left, the different sources in the Middle Eastern region enclosed by Figure 11, are compared on a monthly mean scale between GOME2C and TROPOMI with satisfactory results and correlations ranging between 0.58 and 0.75. Overall, the GOME2C monthly mean VCDs continue to over-estimate the equivalent TROPOMI ones In the equivalent comparisons of the SCD/0.4 levels, right column, the overestimation appears to be nullified, with slopes approaching unity [between 0.91 and 1.08] and correlation coefficients between 0.61 and 0.80.

In Figure 18, comparisons over power plants in South Africa [left] and India [right] also perform well, with slopes nearing 1 and correlations of 0.54 and 0.75 respectively.
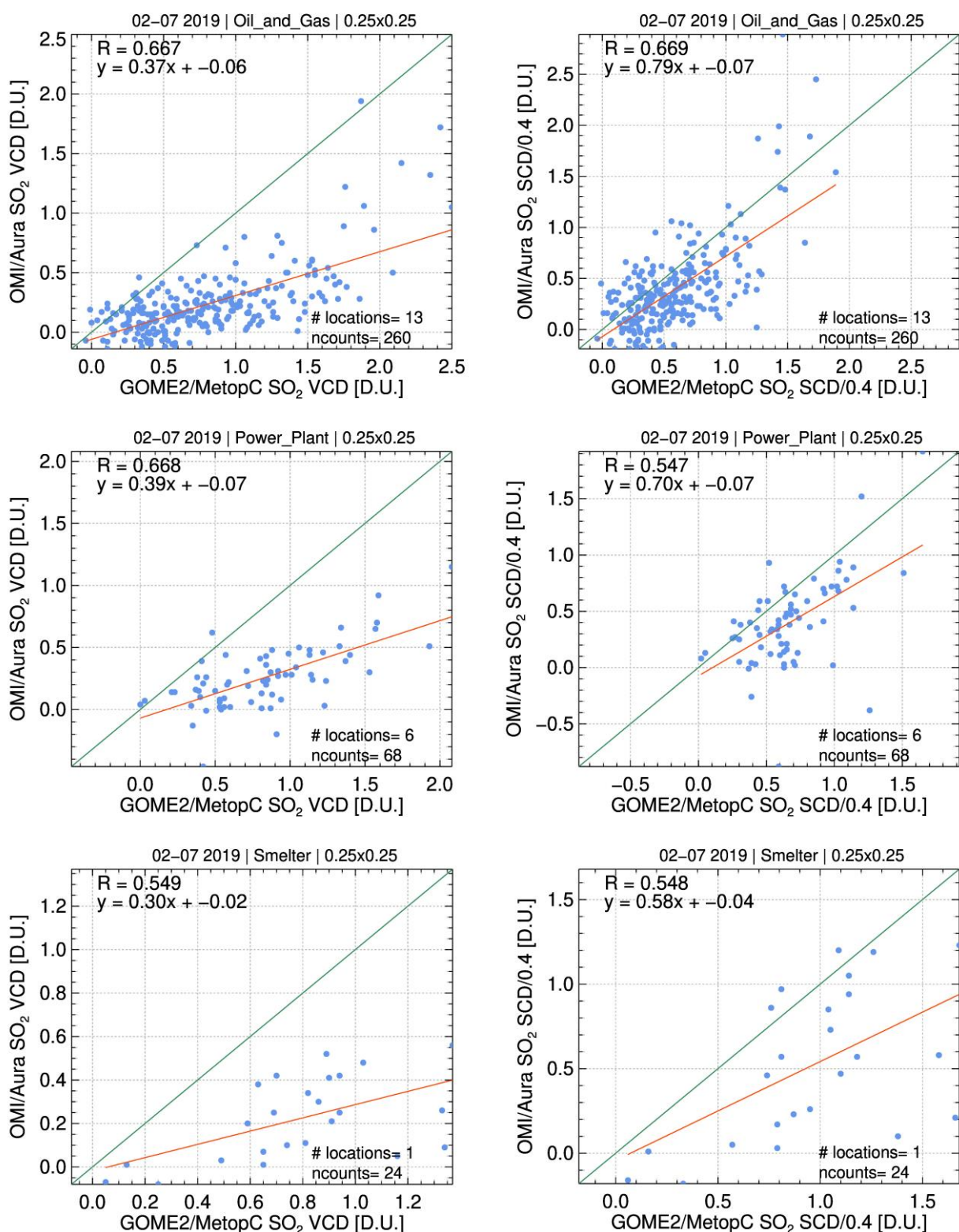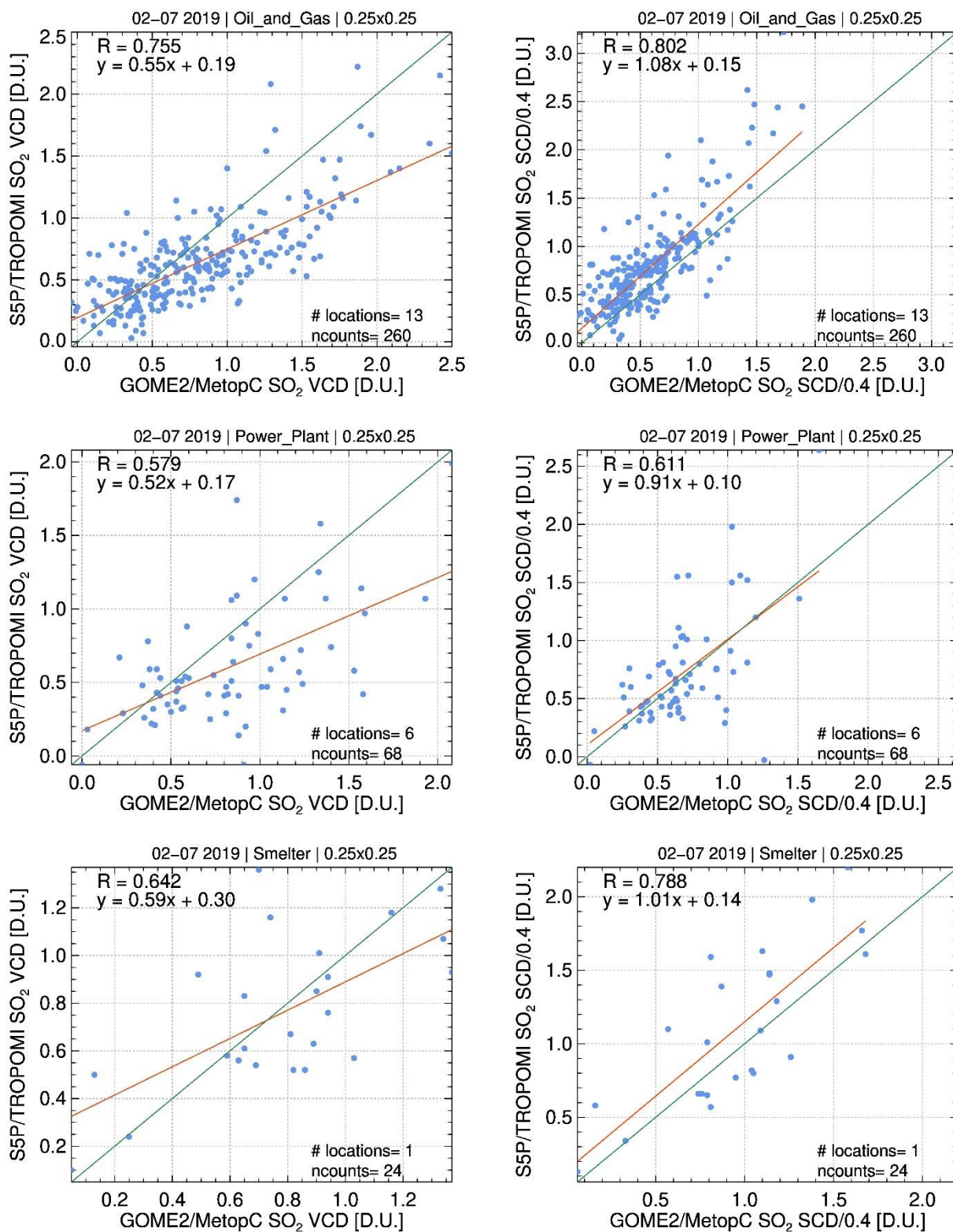
Figure 17. Left. Comparisons of the GOME2C monthly mean SO₂ pollution VCDs for the entire period of February to July 2019 over the Middle Eastern region enclosed by Figure 11, to the TROPOMI VCDs for 13 Oil and Gas sources [upper], 6 Power Plants [middle] and 1 Smelter [lower.] Right. Same for the SCD/0.4 [D.U.] comparisons.
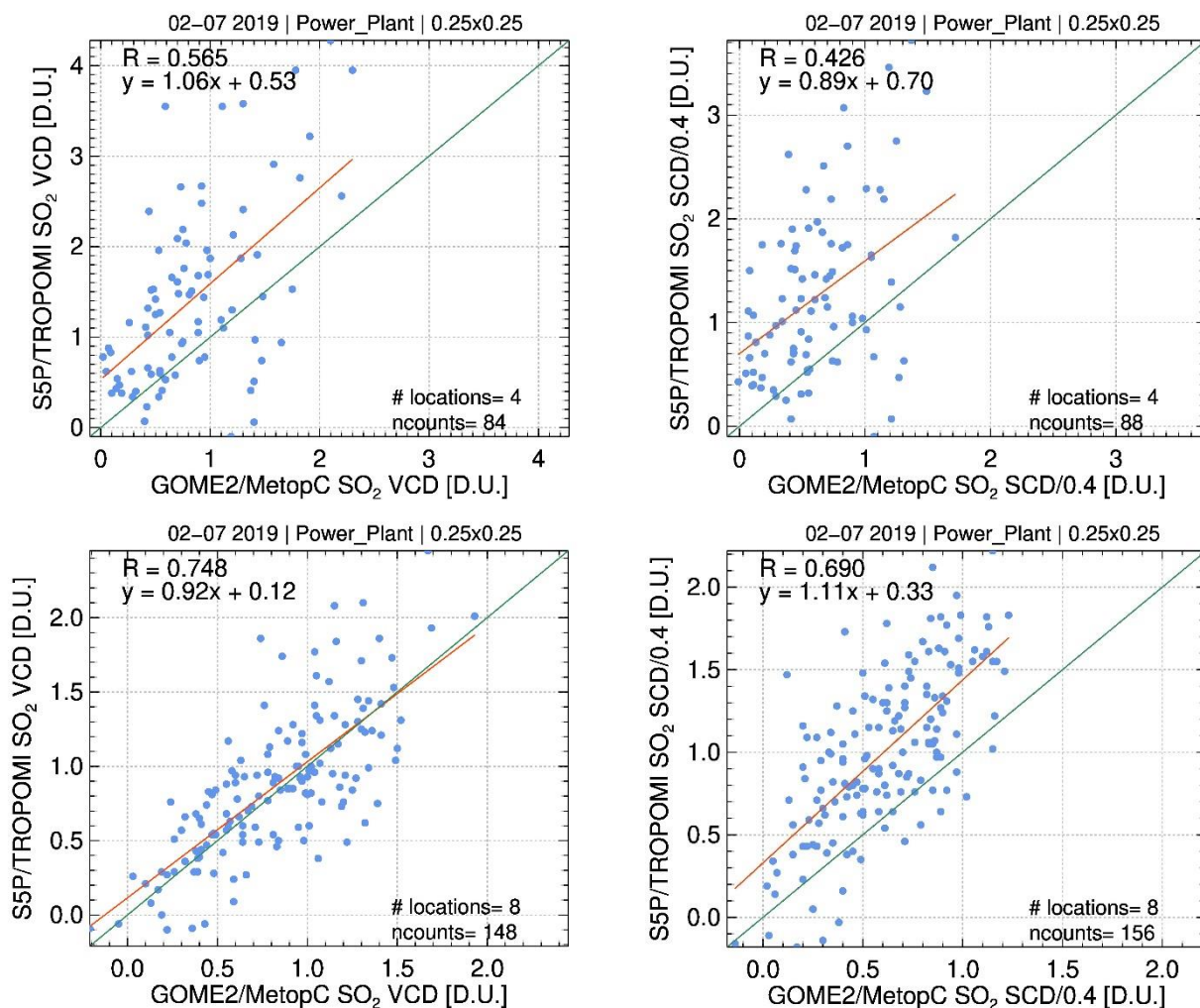
Figure 18. Left. Comparisons of the GOME2C monthly mean SO$_2$ pollution VCDs for the entire period of February to July 2019 over the South Africa region enclosed by Figure 7, top, and over India [20-30°N, 75-90°E], bottom, to the TROPOMI VCDs, for 4 and 8 Power Plant locations respectively. Right. Same for the SCD/0.4 [D.U.] comparisons.

For the cases of the Power Plants over South Africa and India the comparisons on the original VCD levels where very promising with slope and R^2 of 1.06 and 0.57 respectively for the former [Figure 18, upper, left] and 0.92 and 0.75 for the latter [Figure 18, lower, left.] Transforming the SCDs into a comparable quantity, via the division with a common AMF=0.4, [Figure 18, right column] slightly shifts the comparison to higher values for both sensors, while keeping their relative agreement the same.

A similar study was performed on a seasonal basis, separating the six months of the GOME2C dataset into, roughly, spring and summer time, without however any noteworthy different results than those presented for the daily and monthly averages.

On a global scale, examining all monthly mean VCDs for the 44 Power Plants, the 7 Smelters and the 23 Oil and Gas point sources listed in Table 5 to Table 7, we note that **the average difference for the six monthly mean VCDs is ~10%**, the median value ~8%, the minimum difference is -22% and the maximum difference ~+50%. In Table 4 the monthly mean statistics for each of the three different types of sources are shown, with colour coding for easier reading of the different columns.

For the two columns showing the mean VCDs, the colour ranges from white [low SO$_2$ loads] to dark red [high SO$_2$ loads] while for the final column showing their correlation, white/light green colours depict low R^2 values and dark green colours the higher correlations. For the 44 Power plants, the mean GOME2C anthropogenic VCD ranges between 0.50 and 0.77 D.U. while the variability ranges between 0.36 and 0.67 D.U. Very similar loads are provided by the TROPOMI observations with a mean VCD between 0.50 and 0.75 D.U. and variability of 0.43 and 0.74 D.U. The linear correlation coefficient ranges between 0.25 [for July] to 0.64 [for April and May.] For the 7 Smelters, the GOME2C loads range between 0.50 and 0.85 D.U. with variabilities between 0.04 and 0.4 D.U., the TROPOMI loads between 0.44 and 0.99 D.U. and variabilities between 0.33 and 0.73 D.U. and correlations between 0.13 [for May] and 0.92 for February. For the 23 Oil and Gas locations, the GOME2C mean VCDs range between 0.47 and 0.80D.U. and variabilities between 0.26 and 0.56 D.U., the TROPOMI mean VCDs range between 0.47 and 0.65 D.U. and variabilities between 0.30 and 0.42 D.U. and the correlations between 0.46 [April] and 0.86 [July.]

Table 4. Monthly mean statistics for the GOMEC and TROPOMI anthropogenic VCD, and associated std separated by different type of source on a global scale; first block, 44 Power Plants, second block, 7 Smelters and third block, 23 Oil and Gas locations. White/light red colours denote smaller VCD loads and dark red colour higher VCD loads. In the final column, the correlation per month is colour-coded in tones of green in a similar manner.

		GOME2/MetopC		S5P/TROPOMI		
		MEAN [D.U.]	STD	MEAN [D.U.]	STD	Correlation
Power plants	February	0.7669	0.6763	0.7586	0.7203	0.385
[44]	March	0.753	0.3763	0.7354	0.4381	0.2719
	April	0.7009	0.3611	0.6779	0.4561	0.6423
	May	0.6152	0.4416	0.6505	0.7411	0.6409
	June	0.5232	0.3889	0.4803	0.6292	0.6604
	July	0.4928	0.3605	0.499	0.5453	0.2507
Smelters	February	0.6425	0.0457	0.8325	0.3725	0.9191
[7]	March	0.4869	0.3445	0.4494	0.6523	0.317
	April	0.648	0.3579	0.564	0.3426	0.2271
	May	0.5785	0.2321	0.463	0.356	0.137
	June	0.84	0.4531	0.7344	0.6635	0.8355
	July	0.8546	0.4034	0.9917	0.7399	0.5736
Oil and Gas	February	0.6004	0.3632	0.5564	0.3365	0.4791
[23]	March	0.6421	0.4	0.6535	0.4241	0.633
	April	0.4715	0.2601	0.4715	0.2936	0.4633
	May	0.8029	0.5249	0.5796	0.4008	0.7471
	June	0.771	0.5314	0.5199	0.3889	0.7233
	July	0.7919	0.5663	0.5433	0.3956	0.8648
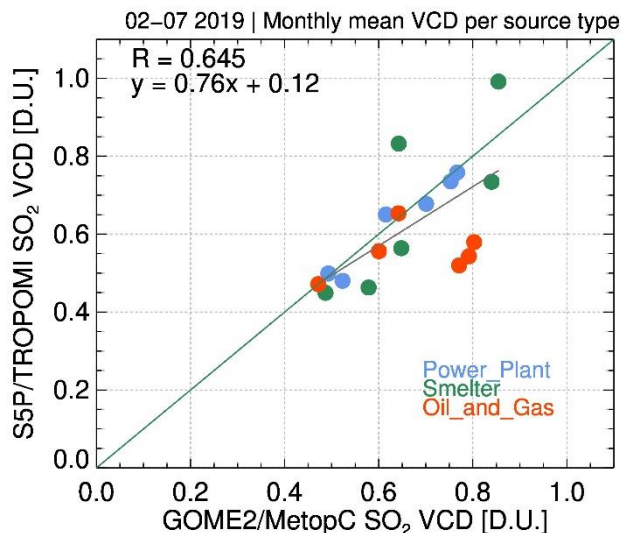
Figure 19. Monthly mean comparison between the GOME2/MetopC monthly mean VCDs [x-axis] and the S5P/TROPOMI monthly mean VCDs [y-axis] for all types of anthropogenic sources, coloured as per the legend.

In Figure 19, a scatter plot for all three different source types, on a monthly mean basis, is provided which shows the overall agreement between GOME2C and TROPOMI, with both sensors reporting similar ranges of SO₂ load and a satisfactory correlation.

We hence conclude that **on a monthly mean basis and over the known anthropogenic sources** the GOME2C anthropogenic VCD product **falls well within the threshold requirement of 100% and, mostly, within the target requirement of 50%.**

3.2.3   Comparison with the MAX-DOAS ground-station at Basrah, Iraq.

The GOME2C anthropogenic SO₂ columns have been compared to MAX-DOAS observations performed at Basrah, Iraq (30.52°N, 47.81°E) for the period April to July 2019. For this exercise, the SO₂ column for the anthropogenic pollution case is chosen. The results are shown in Figure 20, with a timeseries of the comparisons shown in the upper panel and two scatter plots in the lowel panel, depending on the viewing angle of the MAX-DOAS instrument. Overall, the correlation between satellite and ground-based data is rather poor, around 0.4, but the level of SO₂ columns is similar. We note that the comparison is quite difficult because of local SO₂ emissions from refineries.

EUMETSAT
AC SAF

REFERENCE: **SAF/AC/AUTH/VR/SO2**
ISSUE: 11/2020
DATE: 30/11/2010
PAGES: Page **38** of **62**
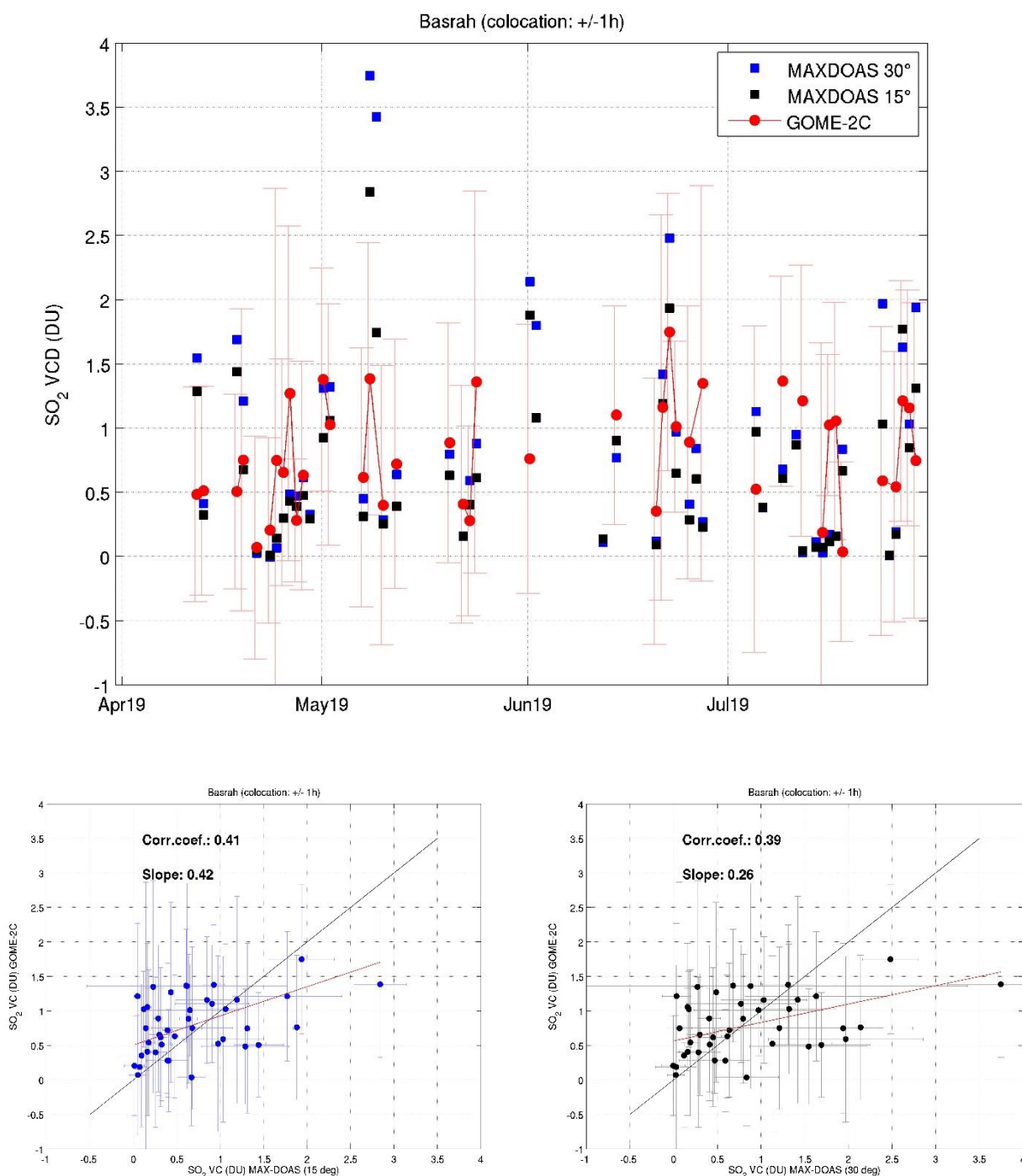
Figure 20. Comparison of daily SO$_2$ columns at Basrah (Iraq) between GOME2C and MAXDOAS measurements. Clear-sky pixels (cloud fractions<30%) are selected within a 100km radius around the station. The ground-based measurements taken 1h around the MetOp-C overpass are averaged for the comparison. Credit: Nayyef Almaliki, Mustafa Aldossary, Ali Almasoudii, Sebastian Donner, Steffen Dörner and Thomas Wagner.

3.2.4 Investigating a more stick SZA filter

The official recommendation for using the SO_2 anthropogenic VCD procured by the GOME2 GPD 4.9 algorithm is filtering out all observations associated with a solar zenith angle greater than 75°. This filter is already included in the SO_2 flag, hence setting that to zero filters out all such pixels. It was however found during this analysis that this filter might require fine tuning, or a selection of a smaller angle as filter criterion. In Figure 21 the effect of the SZA choice in filtering is presented with the month of May 2019 filtered for SZA < 75° is shown in the left and a SZA < 60° in the right. On gross inspection one might state that indeed the dataset does not exhibit the high level of noise when filtered at the edges of the domain. However, when focusing on the region of South Africa (Figure 22) the simple filtering for the higher SZAs produces noise in lower latitudes [between 25° and 30°S] hence hindering the scientific analysis of the hot spots in the country of South Africa.
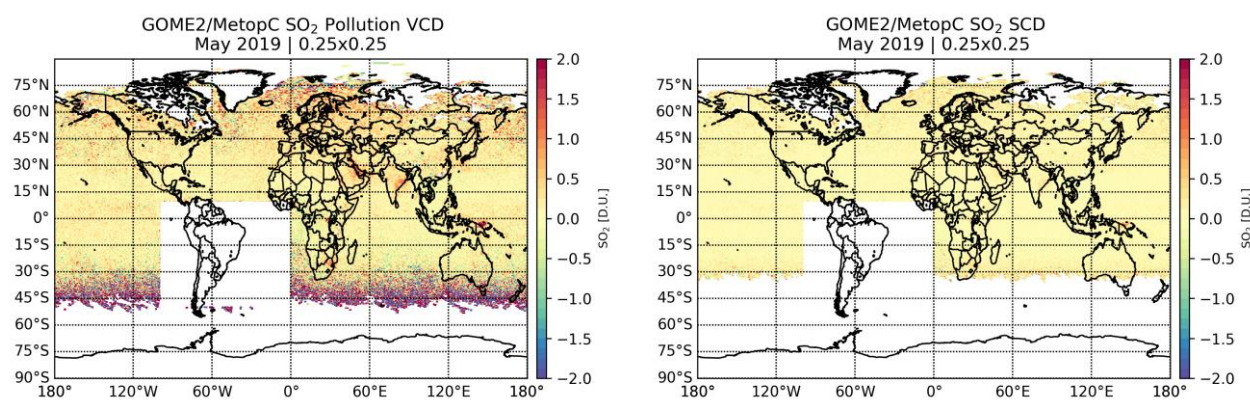
Figure 21. Global gridded GOME2/MetopC SO_2 pollution VCD fields for the month of May 2019 using a SZA lifter of < 75° in the left and a SZA < 60°, in the right plot.
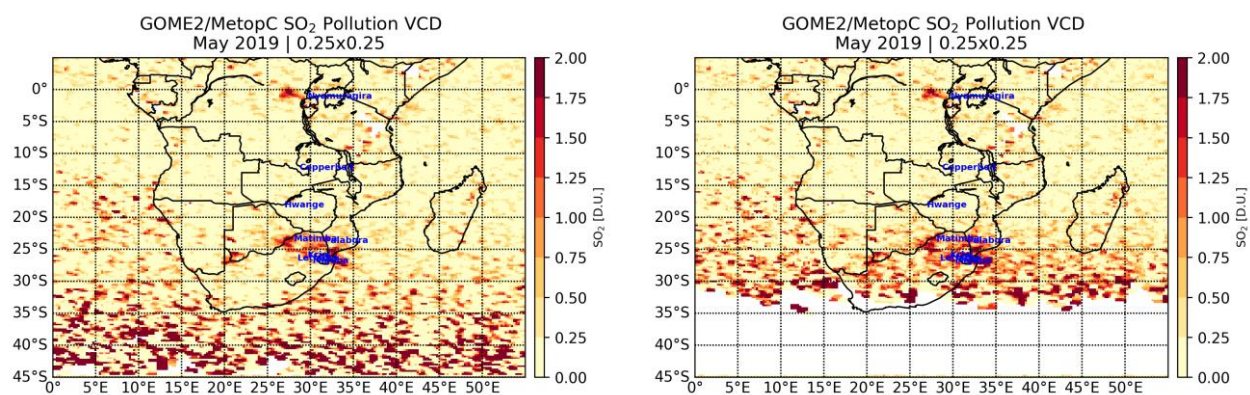
Figure 22. As per Figure 22 zooming into the region of South Africa.
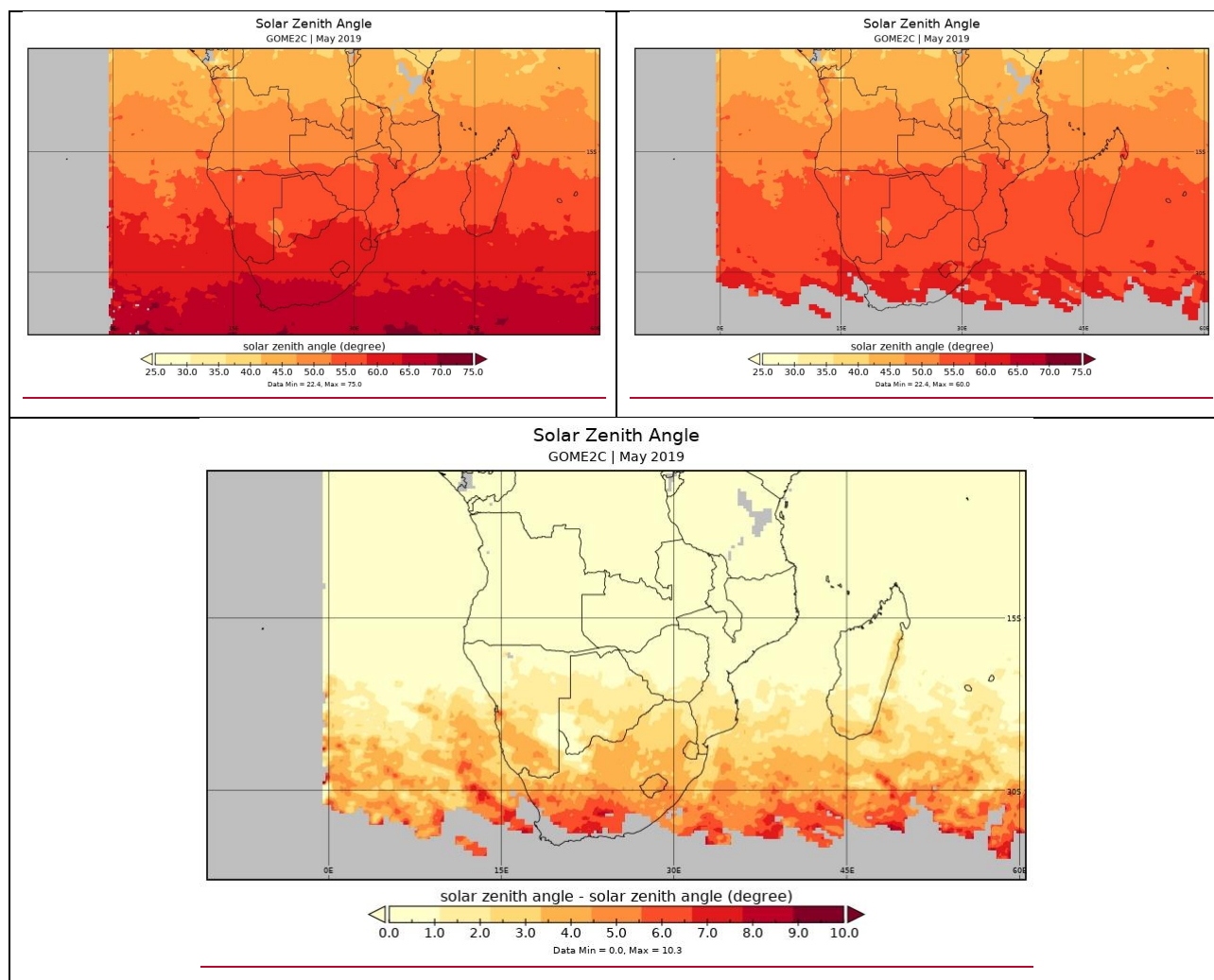
Figure 23. The mean solar zenith angle for GOME2/MetopC for the month of May 2019. Upper left, all observations with associated SZA < 75° are included in the monthly mean. Upper right, all observations with associated SZA < 60° are included in the monthly mean. Lower, the difference in mean angles for the two upper cases. The grey area in the left part of the plot represent data that are filtered for the South Atlantic anomaly and are not accepted as valid.

The explanation of the noise shown in the lower latitudes in Figure 22 is simply one of geometry and is shown pictorially in Figure 23. The mean SZAs associated with the monthly mean VCD of May 2019 are shown in the upper panel, for a cut-off of < 75° on the left and a cut-off of < 60° on the right, with their difference demonstrated in the bottom plot.

It is hence evident that a simple filter in SZA cannot be considered panacea in filtering noisy pixels and a clear message to this fact should be included in the PUM and ReadMe files associated with the GOME2/Metop SO$_2$ products.

3.3   Volcanic SO₂ Vertical Column Density

3.3.1   Comparisons to GOME2/MetopB and S5P/TROPOMI

During the February to July 2019 period of the GOME2C validation dataset, a major eruption of the Raikoke volcano on 21 June occurred in the Kuril Island chain, near the Kamchatka Peninsula in Russia, with SO_2 injection in the UTLS, providing a good test case for the GOME2C product. In the following, we have compared the results assuming an SO_2 plume height of 15km with the corresponding data from GOME-2 MetOp-B (offline SO_2 product) and operational offline S5P/TROPOMI.
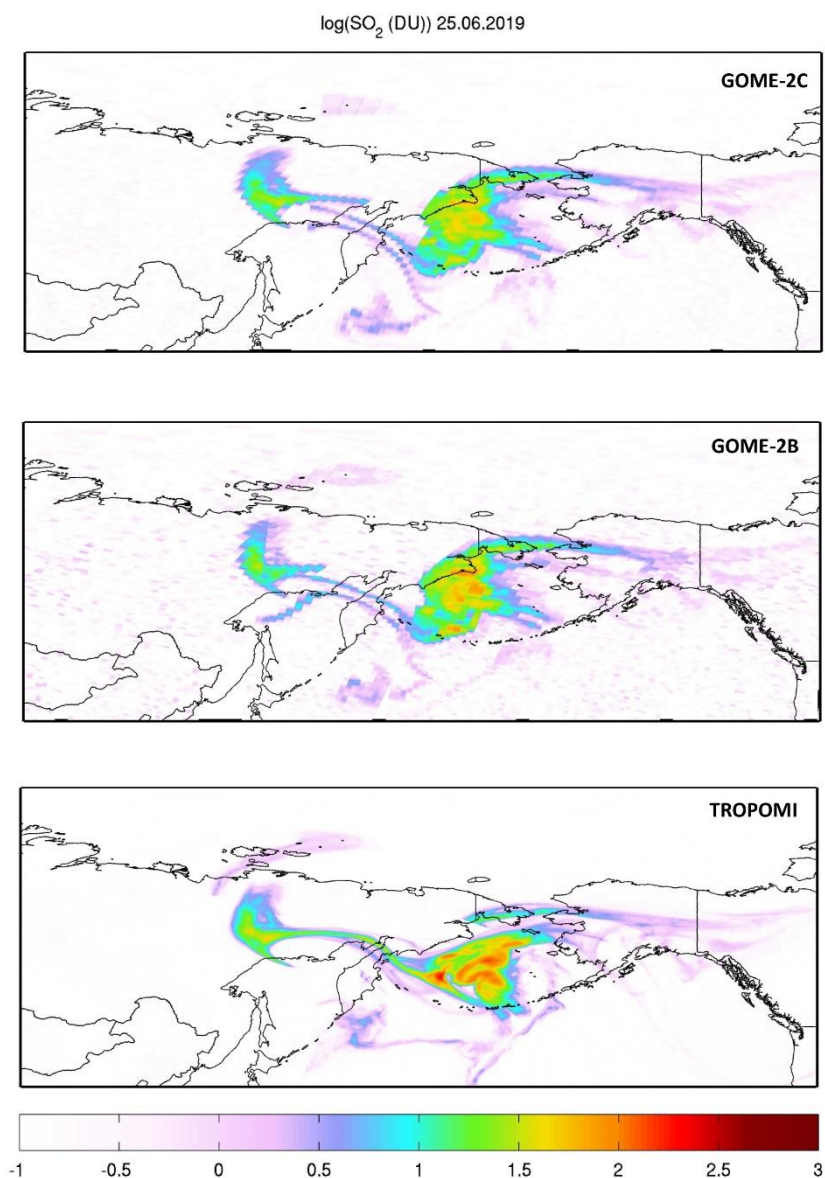
Figure 24. Comparison of SO₂ VCD maps (expressed in logarithmic scale) from (top to bottom) GOME2C, GOME2B and TROPOMI, for the 25th of June 2019 after the Raikoke eruption.

In Figure 24 SO₂ maps from the three instruments on 25 June 2019, 4 days after the start of the eruption, are shown. One can observe that all the three datasets agree qualitatively very well. Despite differences in overpass times, the observed SO₂ patterns are very similar. However, on that day, it is clear that TROPOMI detects higher VCDs (several hundreds of DUs) than GOME2C and GOME2B. This is expected (and has been reported already in previous validation exercises), because the TROPOMI algorithm makes use of different fitting windows to avoid saturation issues while GOME-2 algorithms utilize a single fitting window which is subject to non-linear SO₂ absorption in case of high SO₂ loadings. From Figure 24, one can also note that GOME2-C results are less noisy than GOME2B and the likely explanation is a difference in the fitting window used: GOME2C fits SO₂ in the 312-326nm range which stabilize the DOAS fits compared to the 315-326nm interval used for GOME2B. We also note that for the core of the SO₂ plume, GOME2C VCDs tend to be lower than GOME2B results. Again, this is likely due the change in fitting interval: the inclusion of the strong SO₂ absorption band around 313 nm makes the 312-326nm more sensitive to non-linear effects than the 315-326 nm range.
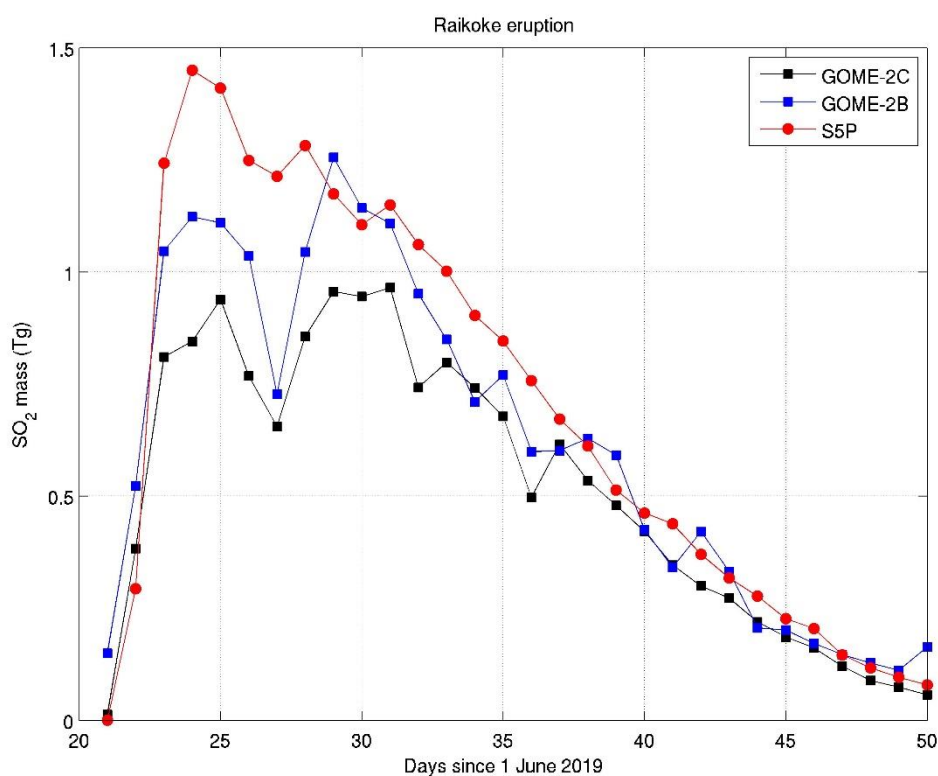
Figure 25. Comparison of SO₂ total mass (expressed in Tg) from GOME2C, GOME2B and TROPOMI, for one month after the Raikoke eruption. The values are calculated by gridding the data at a 0.1°x0.1° resolution and selecting the grid cells with SO2 VCDs > 1 DU for the Northern hemisphere. It should be stressed that because the SO₂ plume was located near 180° longitude there are measurements for a given orbit that belong to two calendar days and this is the likely explanation for some of the day-to-day variations in the time-series.

Figure 25 compares estimations of the total SO₂ mass for one month after the eruption of Raikoke from the three instruments. In general, TROPOMI detects higher SO₂ mass (up to ~1.5 Tg) than GOME2B. GOME2C is even smaller, as a result of the non-linear effects (stronger for the 312-326 nm). In July, the GOME2C, GOME2B and TROPOMI estimates are reasonably close. To further

investigate the agreement between GOME2C and GOME2B, Figure 26 shows a comparison of SO$_2$ VCDs for Raikoke for the first half of July. As can be seen, for high columns (~50DU) measured by GOME2B, the GOME2C results are up to 30% lower. This is to some extend expected from the change in fitting window. For low SO2 VCDs, GOME2C tends to underestimate the GOME2B SO$_2$ columns by about 7-15%. Although this difference is acceptable, the reason is not completely clear but might be due to the effect of ozone absorption on the SO$_2$ AMF that has not fully accounted for. The already demonstrated differences in the SCDs between the GOME2 instruments [Section 3.1] should also not be discounted.
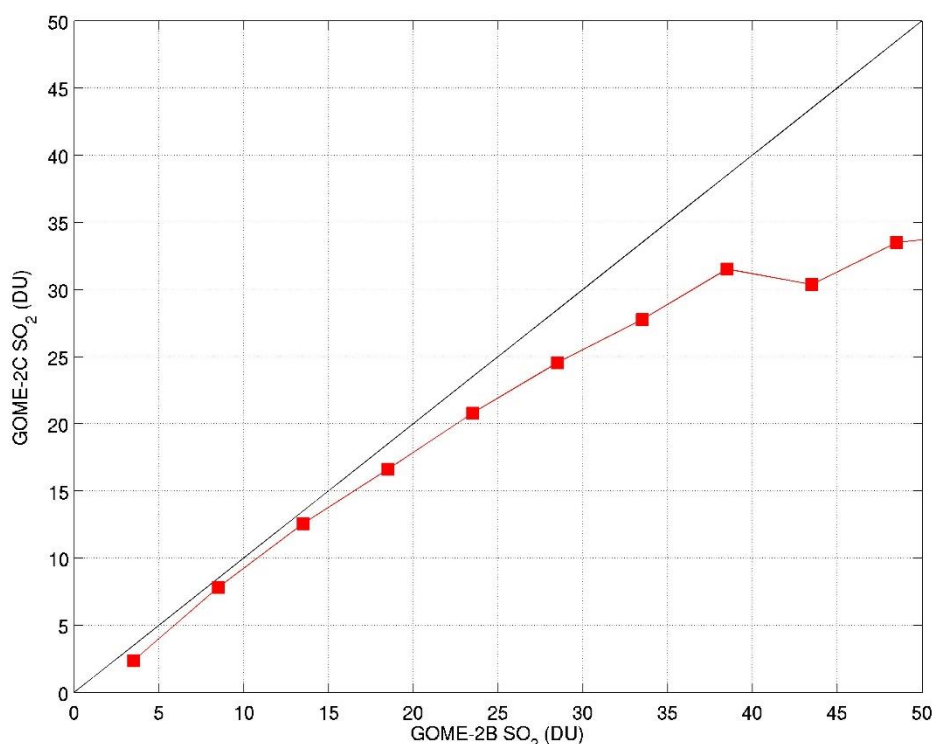
Figure 26. Comparison of SO$_2$ VCD (in DU) from GOME2C and GOME2B, for 1-15 July 2019 after the Raikoke eruption. The values are calculated by gridding the data at a 0.1°x0.1° resolution with SO$_2$ VCDs > 1 DU for the Northern hemisphere. The GOME2C VCDs are averaged for a fixed GOME2B SO$_2$ VCD grid.

3.3.2 Comparisons to BIRA-IASB zenith-sky data

In the following subsection, we compare the SO$_2$ L2 volcanic dataset from GOME-2 onboard MetOp-C to ground-based zenith-sky data from BIRA-IASB stations, covering the 6 months of available data, from February to July 2019. During this period of time, a few eruptions with During this period of time, few eruptions with SO$_2$ injection in the UTLS took place, including the Raikoke eruption on 21 June (near the Kamchatka Peninsula in Russia), that travelled in the Northern Hemisphere for about a month, and the Ubinas eruption on 19/7/2019, (Perou) that travelled around the Southern Hemisphere.

Several BIRA-IASB stations (http://uv-vis.aeronomie.be/groundbased/stations) cover the available datasets time-period, namely:

- **Harestua** (60.2°N, 10.75°E, **Norway**): BIRA-IASB is measuring in ZenithSky geometry since the '90 and with an updated instrument since November 2012 (Hendrick et al., 2007);
- **Uccle** (50,5°N, 4°E, **Belgium**): BIRA-IASB measured with a MAXDOAS instrument from end January 2017 to March 2020 (Dimitropoulou et al., 2020);
- **Jungfraujoch** (46.5°N, 7.98°E, **Switzerland**): BIRA-IASB is measuring in MAXDOAS geometry since 2010 (Hendrick et al, 2012);
- **Xianghe** (39.75°N, 116.96°E, **China**): BIRA-IASB is measuring with a MAXDOAS (Clémer et al., 2010; Hendrick et al, 2014) since 2010, with an instrumental gap from July 2018 to November 2019, leading to only zenith-sky measurements during that period;
- **Reunion** (21°S, 55°E, **Reunion Island**): BIRA-IASB measured between April 2016 and January 2018 with a MAXDOAS in LePort, on the coast, and then moved the instrument to the Maido site (at 2360m) and is measuring there since June 2018.

The **Bujumbura** station (3°S, 29°E, **Burundi**, Gielen et al., 2017, measuring since 11/2013), is temporarily off during the available GOME2C time-period, due to instrumental problems.

GOME2C SO_2 data have been extracted in a radius of 150km around these 5 ground-based stations and the time-series of the VCD data at 1.5km, 2.5km and 15km are presented in Figure 27. It can be seen that the SO_2 dataset is quite noisy for the SO_2 VCD data at 1km and 2.5km , while volcanic SO_2 at 15km is less noisy. Only 3 stations have an interesting SO_2 VCD signal at 15km to look to in detail: Uccle and Jungfraujoch for Raikoke eruption (https://volcano.si.edu/volcano.cfm?vn=290250&vtab=Weekly) with its plume travelling over Europe in mid July (see Figure 28), and Reunion Island with the Ubinas eruption plume (https://volcano.si.edu/showreport.cfm?doi=GVP.WVAR20190724-354020) passing close to the island on 23 July Figure 28(see Figure 29). Unfortunately, an instrumental problem occurred in Jungfraujoch in June 2019, and ground-based data only up to the 10th June 2019 are available, reducing the stations of interest to two, Uccle and Reunion. GOME-2 data are further filtered for SZA<70°.
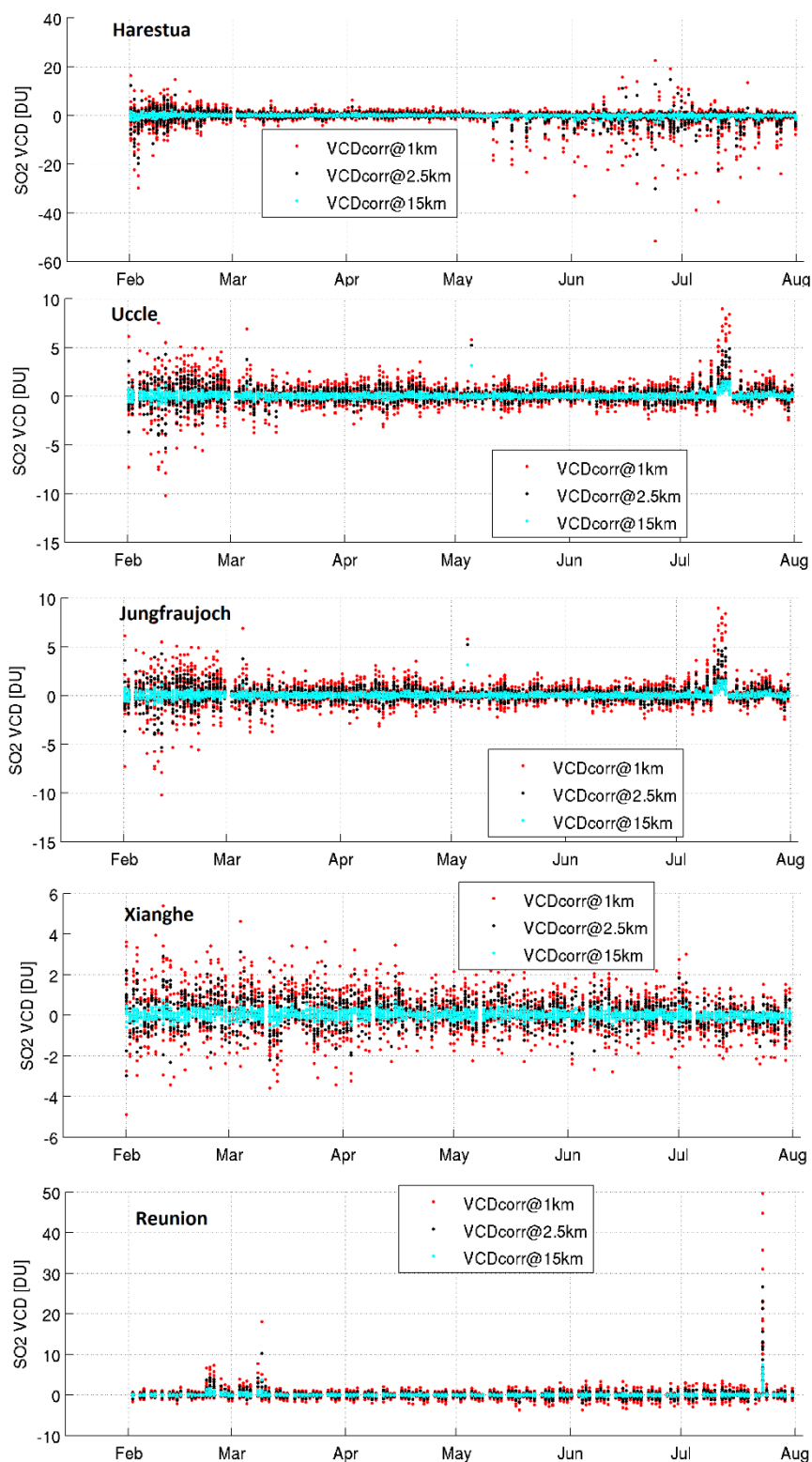
Figure 27. GOME2C SO$_2$ VCD time series of all pixels within 150km radius around the ground-based BIRA-IASB stations, for February to July 2019; the anthropogenic pollution at 1km in red, the anthropogenic pollution at 2.5km in black and the volcanic load at 15km in cyan.

SO_2 analysis are not performed routinely, and only the time-periods around July have been analysed from the BIRA-IASB ground-instruments, in order to compare to GOME2C. The ground-based spectra have been analysed using the DOAS settings specified in Wang et al., 2014 (analysis in the 305-317.5 nm window) with a fixed reference spectrum close to the period of interest (on a day not affected by the eruption). The slant columns measured at zenith are used to estimate the stratospheric SO_2 content by using a geometrical stratospheric AMF that depends only on the solar zenith angle (Honninger et al., 2004):

$$AMF_{strato} = 1/\cos(SZA) \tag{1}$$

For large stratospheric eruptions, both MAXDOAS and ZenithSky instruments are sensitive to the SO_2 in the stratosphere, and the stratospheric SO_2 content is obtained as:

$$VCD_{strato} = DSCD_{zenith}/AMF_{strato} \tag{2}$$

Only ground-based VCD below 60° SZA and with RMS < 0.02 are considered to reduce uncertainty on the ground-based data analysis.
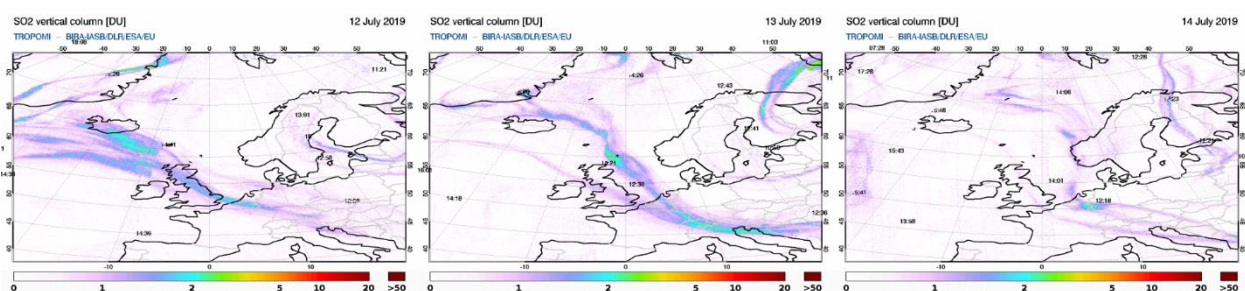
Figure 28. Illustration of the TROPOMI volcanic SO_2 VCDs over Europe between the 12th and 14th July 2019, as presented in the SACS webpage.
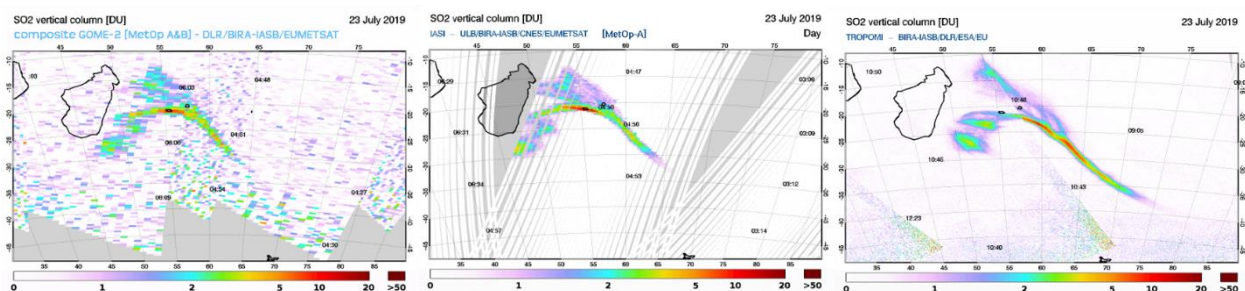
Figure 29. Illustration of the Ubinas eruption plume, as seen in the SACS webpage by GOME2A&B, IASI and TROPOMI on the 23th of July 2019.

3.3.2.1   Comparison over the Uccle station | Raikoke eruption

In the following section the comparisons over Uccle between the zenith-sky data and GOME2C are shown for the Raikoke eruption starting on the 6th of July and up to the 14th of July. The latter are considered only for pixels within 80km from the station. Zenith-sky data from Uccle are analyzed with a reference spectra taken on the 3rd of July, before the arrival of the Raikoke plume. For additional illustration, the S5p/TROPOMI SO_2 data have also been extracted within 20km around the Uccle station, and SO_2 VCD columns estimated at 15km are also considered in the following comparison figures. It can be seen that small columns (smaller than 1 DU) are obtained in the first days (6 to 11 July, shown in Figure 30 and Figure S 1 to Figure S 6 of the Appendix), while larger signal is seen from 12 July to 14 July (Figure 31 and Figure S 7 to Figure S 8). An overview of the whole time-period is given in Figure 32.
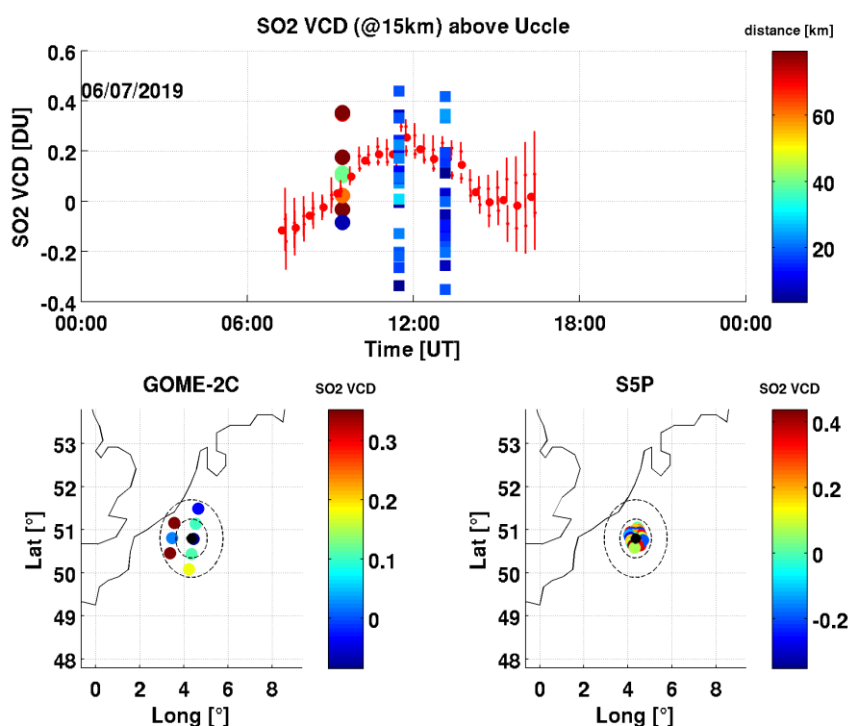
Figure 30. SO_2 VCD comparisons above Uccle on 6 July 2019. Red dots are the ground-based data (small dots: all the measurements from zenith-sky, larger dots: hourly averages), while colored dots are GOME2C VCD at 15km color-coded as a function of the distance in the upper plot, and as a function of the VCD on the lower maps. TROPOMI SO_2 VCD at 15km are also given as squared markers. The dashed circles in the maps present 50km and 100km-radius circles around the ground-based station.
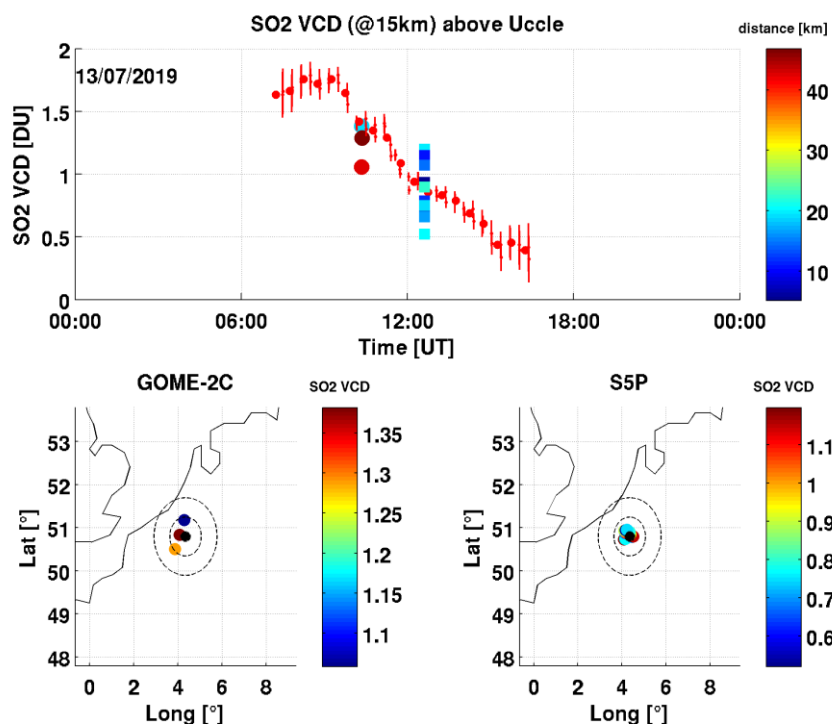
Figure 31. As Figure 30, for Uccle on the 13th of July 2019.
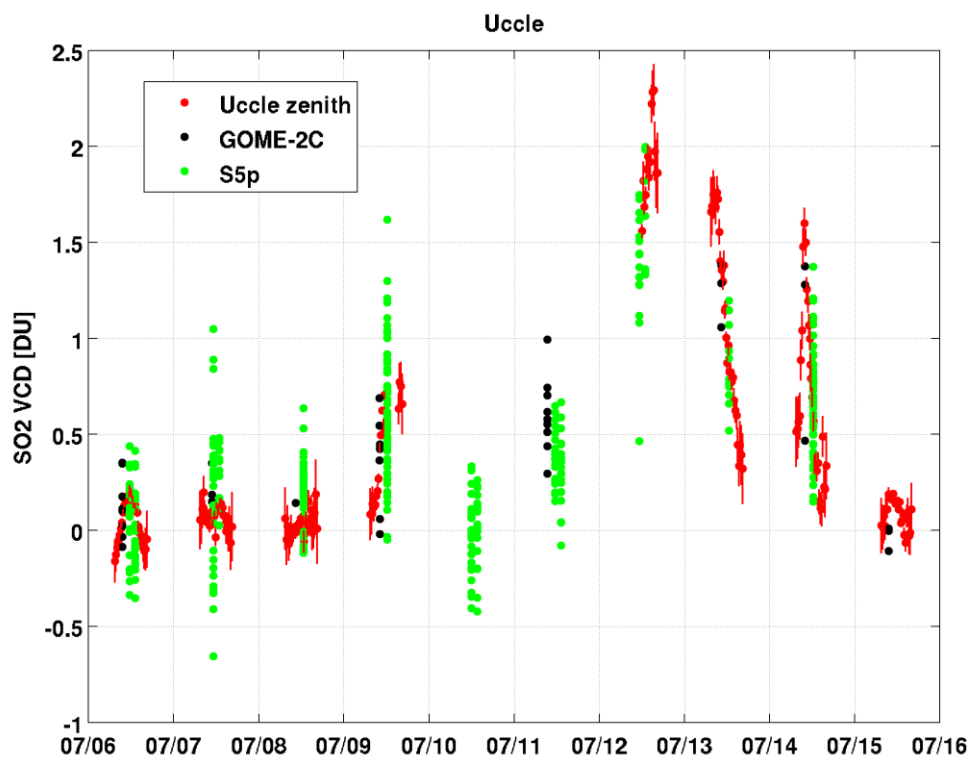
Figure 32. Overview of the time-series of SO₂ VCD around Uccle from 6 to 16 July 2019, with ground-based zenith-sky data (red), GOME2C (black) and S5p/TROPOMI (green) data.

3.3.2.2 Comparison over the Reunion station | Ubinas eruption

For Reunion Island, the period around 23 July has been analysed for the ground-based data, with a reference spectra taken on the 20 July. A clear SO$_2$ signal is only found on the 23 July (Figure 33), confirming the rapid travel of the Ubinas volcanic plume, starting from South America and reaching East of Africa in a week. Comparisons on the 23 July are presented in Figure 34, showing the strong decrease of SO$_2$ between the morning GOME2C overpass to the early afternoon TROPOMI overpass, as also seen by the ground-based zenith-sky data.
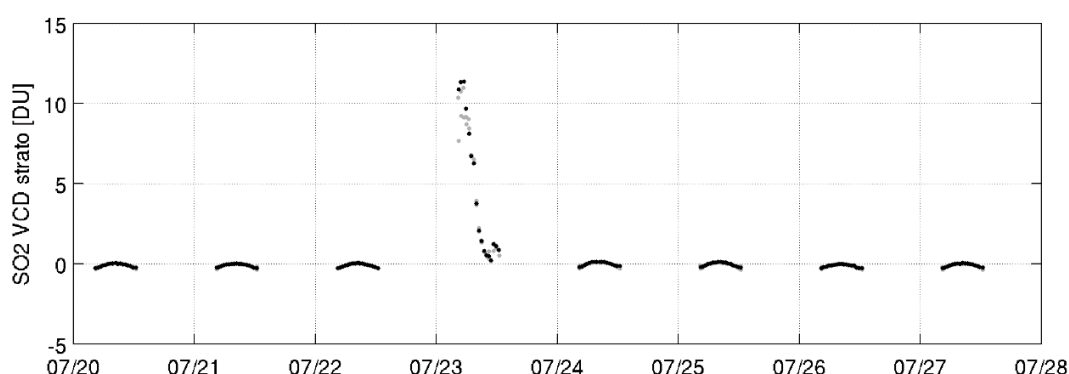
Figure 33. Reunion Maido SO$_2$ VCD data in July 2019.
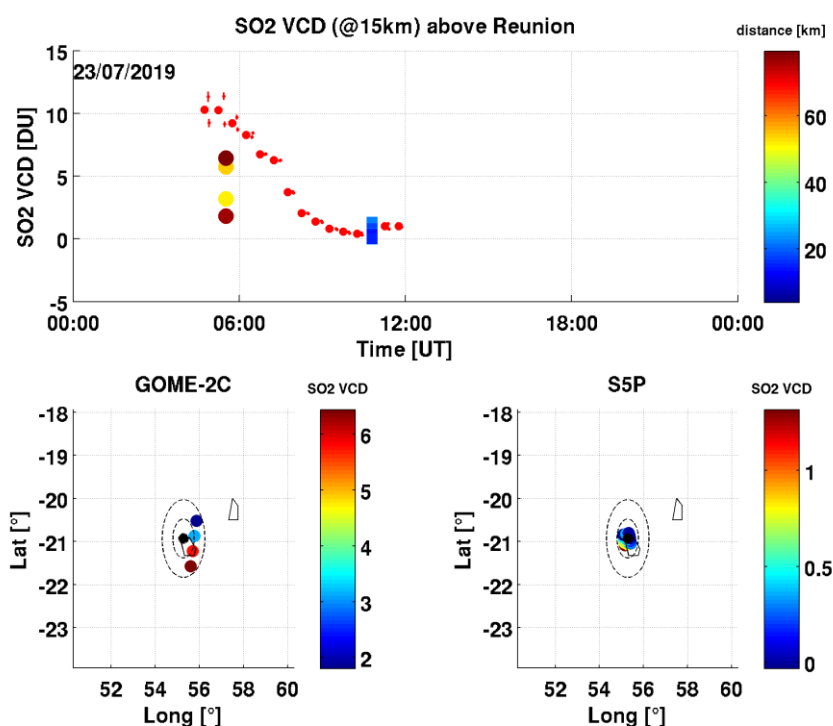
Figure 34. SO$_2$ VCD comparisons above Reunion (Maido) on 23 July 2019. Red dots are the ground-based data (small dots: all the measurements from zenith-sky, larger dots: hourly averages), while colored dots are GOME2C VCD at 15km color-coded as a function of the distance in the upper plot, and as a function of the VCD on the lower maps. TROPOMI SO$_2$ VCD at 15km are also given as squared markers.

4 CONCLUSIONS

In this report, we present the assessment of the GOME2/MetopC anthropogenic and volcanic SO$_2$ total columns reported by the operational GDP4.9 algorithm. The two main differences to the GDP4.8 algorithm, currently used on the GOME2/MetopA and /MetopB instruments, is the update of the SO$_2$ absorption cross-sections and the usa~~ge~~ of a wider wavelength range for the SO$_2$ retrieval. Issues with the L1b radiances have been identified for both GOME2A and GOME2B instruments which do not permit an easy evaluation of any algorithm changes among the three sister instruments.~~Issues with the L1b radiances have been identified for both GOME2A and GOME2B instruments which do not permit an easy evaluation as to these algorithm changes among the three sister instruments.~~

The threshold requirement for the accuracy of the GOME2/MetopC SO$_2$ columns has been set to 100%, the target requirement for solar zenith angles smaller than 70° was set to 50% and the optimal accuracy at 30%. In order to assess the accuracy level of the provided columns we have used inter-satellite comparisons, ~~and~~ namely against OMI/Aura and S5P/TROPOMI, as well as comparisons against MAX-DOAS ground-based instruments, for both anthropogenic and volcanic SO$_2$ columns, for a time period between February and July 2019. Summarizing:

Anthropogenic SO$_2$ signal:

- On a monthly mean temporal choice and a 0.25x0.25°spatial choice, the GOME2C VCDs show very similar levels to the ones reported by S5P/TROPOMI over known hot-spots. On a global scale examining all monthly mean VCDs for the 44 Power Plants, the 7 Smelters and the 23 Oil and Gas point sources listed in Table 5 to Table 7, we note that **the average difference for the six monthly mean VCDs is ~10%**, the median value ~8%, the minimum difference is -22% and the maximum difference ~+50%. Satisfactory agreement is thus found with correlation coefficients ranging between 0.5 and 0.8, depending on the month [i.e. season] and the strength of the known hot-spot source. The GOME2C VCD fields beyond the locations of the hot-spots is quite noisy and require filtering. See relevant detailed Section 3.2.2.3.
- On a monthly mean temporal choice and a 0.25x0.25°spatial choice, the GOME2C VCDs show higher levels to the ones reported by OMI/Aura over known hot-spots. The OMI/Aura fields are seemingly without any noise but also provide values smaller by approximately half for the VCD levels~~s~~ compared to both GOME2C and TROPOMI. Irrespectively, satisfactory agreement is found with correlation coefficients ranging between 0.55 and 0.7, depending on the month [i.e. season] and the strength of the known hot-spot source. Comparing the SCDs, divided with a common AMF factor, further demonstrates that GOME2C is varying in a similar way as OMI, even though the absolute VCD values and ranges do not correspond~~Comparing the SCDs, divided with a common AMF factor, further demonstrates of how GOME2C is varying in a similar manner as OMI, even though the absolute VCD values and ranges do not correspond~~. See relevant Section 3.2.1
- As daily means ~~On a daily temporal choice~~ and~~,~~ either per known and strong hot-spots of anthropogenic SO$_2$ or per area average enclosing known and strong hot-spots of anthropogenic SO$_2$, the correlations between GOME2C and TROPOMI VCDs and SCDs vary between 0.3 and 0.45.

This is one of many indications that, at a daily temporal scale, the GOME2C VCDs are not sufficiently sensitive to the very localized SO$_2$ emissions. See relevant Sections 3.2.2.1 and 3.2.2.2.

- Excluding the location around a known hotspots, the GOME2 SO$_2$ VCDs below 30°S are too noise-ridden to be usable. Since the GOME2C dataset we had a our disposal was for autumn and winter-time of the Southern Hemisphere, we postulate that this elevated noise is due both to the higher SZAs and also the absence of SO$_2$ sources. (relevant Section 3.1.) Furthermore, Wwe recommend a sticker SZA filter for the dataset, at 60°, to be implemented in the SO2_flag in the next release of reprocessed GOME2/Metop SO$_2$ data and a clear message of all the implications discussed in Section 3.2.4 be included in the PUM and ReadMe files associated with the product.

- Validation at the Bashrah MAX-DOAS station shows rather poor correlation between satellite and ground-based 1h temporally collocated data (around 0.4) albeit with similar SO$_2$ columnar levels. We should note however that the comparisons are hindered by multiple local sources in the Middle East [refineries, power plants, and so on.] See relevant Section 3.2.3.

Volcanic SO$_2$ signal for the Raikoke and Ubinas eruptions:

- For the Raikoke June 23rd eruption and subsequent transport of the SO$_2$ plume round the Northern Hemisphere, the GOME2C VCDs were compared against both GOME2B and TROPOMI volcanic fields. Overall, GOME2C captures well both the location and the relative spread of the Raikoke volcanic plume, see Section 3.3.1.

- TROPOMI detects higher VCDs (several hundreds of DUs) than GOME2C and GOME2B. This can is quitebe expected as the TROPOMI algorithm uses different fitting windows to avoid saturation issues while both GOME2 GDP4.8 and GDP4.9 algorithms utilize a single fitting window which is subject to non-linear SO$_2$ absorption in case of high SO$_2$ loadings, see Section 3.3.1.

- The GOME2C VCD maps are less noisy than GOME2B and the likely explanation is the already reported difference in the fitting window used: GOME2C fits SO$_2$ in the 312-326nm range which stabilizes the DOAS fits compared to the 315-326nm interval used for GOME2B. We also note that for the core of the SO$_2$ plume, GOME2C VCDs tend to be lower than GOME2B results. Again, this is likely due the change in fitting interval: the inclusion of the strong SO$_2$ absorption band around 313 nm makes the 312-326nm more sensitive to non-linear effects than the 315-326 nm range (Section 3.3.1).

- For high columns [~50 D.U.] reported by GOME2B, the GOME2C VCDs were found to be up to 30% lower. This is to some extentd expected from the change in fitting window. For low SO$_2$ volcanic VCDs, GOME2C tends to underestimate the GOME2B SO$_2$ columns by about 7-15%. Although this difference is acceptable and well within the target threshold criteria, the reason is not completely clear but might be due to the effect of ozone absorption on the SO$_2$ AMF that has not fully accounted for (Section 3.3.1).

- For the Raikoke and the Ubinas eruptions, comparisons were also carried out against BIRA zenith sky ground-based observations. Although the relatively small number of coincident cases (only 2 stations, with one and eight days respectively), the ground-based stations generally show enhanced SO$_2$ signals of similar order of magnitude as do the GOME2C and TROPOMI SO$_2$ overpasses, see Sections 3.3.2.1 and 3.3.2.2.

We hence conclude that the GOME2/MetopC anthropogenic and volcanic product is able to capture the emissions from these different types of activities on a monthly mean temporal scale and after

careful screening for cloudiness, high solar zenith angles and conflicting sources, **within the target accuracy criterion of 50%.** For the case of the anthropogenic SO_2 field this target accuracy is achieved on a monthly mean temporal scales over low and medium - or spread out spatially – sources and daily temporal scales over the stronger emission sources. For the case of the volcanic SO_2 field, the stronger eruptions are well captured, and within target accuracy, by the GOME2/MetopC product on a daily scale.

REFERENCES

Birk, Manfred, & Wagner, Georg. (2018). ESA SEOM-IAS – Measurement and ACS database SO₂ UV region (Version 1) [Data set]. Zenodo. http://doi.org/10.5281/zenodo.1492582

Bogumil, K., Orphal, J., Homann, T. Voigt, S., Spietz, P., Fleischmann, O. C., Vogel, A., Hartmann, M., Bovensmann, H., Frerik, J., and J.P. Burrows (2003), Measurements of Molecular Absorption Spectra with the SCIAMACHY Pre-Flight Model: Instrument Characterization and Reference Data for Atmospheric Remote-Sensing in the 230-2380 nm Region, J.Photochem. Photobiol. A.,157, 167- 184.

Clemer, K., Van Roozendael, M., Fayt, C., Hendrick, F., Hermans, C., Pinardi, G., Spurr, R., Wang, P., and De Maziere, M.: Multiple wavelength retrieval of tropospheric aerosol optical properties from MAXDOAS measurements in Beijing, Atmos. Meas. Tech., 3, 863-878, 2010.

Dimitropoulou, E., Hendrick, F., Pinardi, G., Friedrich, M. M., Merlaud, A., Tack, F., De Longueville, H., Fayt, C., Hermans, C., Laffineur, Q., Fierens, F., and Van Roozendael, M.: Validation of TROPOMI tropospheric NO2 columns using dual-scan MAX-DOAS measurements in Uccle, Brussels, Atmos. Meas. Tech. Discuss., https://doi.org/10.5194/amt-2020-33, in review, 2020.

Fioletov, V., McLinden, C. A., Griffin, D., Theys, N., Loyola, D. G., Hedelt, P., Krotkov, N. A., and Li, C.: Anthropogenic and volcanic point source SO2 emissions derived from TROPOMI on board Sentinel-5 Precursor: first results, Atmos. Chem. Phys., 20, 5591–5607, https://doi.org/10.5194/acp-20-5591-2020, 2020.

Gielen, C., Hendrick, F., Pinardi, G., De Smedt, I., Fayt, C., Hermans, C., Stavrakou, T., Bauwens, M., Muller, J.-F., Ndenzako, E., Nzohabonayo, P., Akimana, R., Niyonzima, S., Van Roozendael, M., and De Maziere, M.: Characterisation of Central-African aerosol and trace-gas emissions based on MAX-DOAS measurements and model simulations over Bujumbura, Burundi, Atmos. Chem. Phys. Discuss., doi:10.5194/acp-2016-1104, in review, 2017.

Hendrick, F., Mahieu, E., Bodeker, G. E., Boersma, K. F., Chipperfield, M. P., De Mazière, M., De Smedt, I., Demoulin, P., Fayt, C., Hermans, C., Kreher, K., Lejeune, B., Pinardi, G., Servais, C., Stübi, R., van der A, R., Vernier, J.-P. and Van Roozendael, M.: Analysis of stratospheric NO2 trends above Jungfraujoch using ground-based UV-visible, FTIR, and satellite nadir observations, Atmos. Chem. Phys., 12(18), 8851–8864, doi:10.5194/acp-12-8851-2012, 2012.

Hendrick, F., Muller, J.-F., Clamer, K., Wang, P., De Maziere, M., Fayt, C., Gielen, C., Hermans, C., Ma, J. Z., Pinardi, G., Stavrakou, T., Vlemmix, T., and Van Roozendael, M.: Four years of ground-based MAX-DOAS observations of HONO and NO2 in the Beijing area, Atmos. Chem. Phys., 14, 765-781, doi:10.5194/acp-14-765-2014, 2014.

Hendrick, F., Van Roozendael, M., Chipperfield, M. P., Dorf, M., Goutail, F., Yang, X., Fayt, C., Hermans, C., Pfeilsticker, K., Pommereau, J.-P., Pyle, J. A., Theys, N., and De Maziere, M.: Retrieval of stratospheric and tropospheric BrO profiles and columns using ground-based zenith-sky DOAS observations at Harestua, 60° N, Atmos. Chem. Phys., 7, 4869-4885, doi:10.5194/acp-7-4869-2007, 2007.

Honninger, G., von Friedeburg, C. and Platt, U.: Multi axis differential optical absorption spectroscopy (MAX-DOAS), Atmos. Chem. Phys., 4, 231–254 [online] Available from: www.atmos-chem-phys.org/acp/4/231/, 2004.

Li, C., Krotkov, N. A., Leonard, P. J. T., Carn, S., Joiner, J., Spurr, R. J. D., and Vasilkov, A.: Version 2 Ozone Monitoring Instrument SO2 Product (OMSO2 V2): New Anthropogenic SO2 Vertical

Column Density Dataset, Atmos. Meas. Tech. Discuss., https://doi.org/10.5194/amt-2020-186, in review, 2020a.

Li, Can, Nickolay A. Krotkov, and Peter Leonard (2020b), OMI/Aura Sulfur Dioxide (SO$_2$) Total Column L3 1 day Best Pixel in 0.25 degree x 0.25 degree V3, Greenbelt, MD, USA, Goddard Earth Sciences Data and Information Services Center (GES DISC), Accessed: 16.11.2020], 10.5067/Aura/OMI/DATA3008

Wang, T., Hendrick, F., Wang, P., Tang, G., Clémer, K., Yu, H., Fayt, C., Hermans, C., Gielen, C., Müller, J.-F., Pinardi, G., Theys, N., Brenot, H. and Van Roozendael, M.: Evaluation of tropospheric SO2 retrieved from MAX-DOAS measurements in Xianghe, China, Atmos. Chem. Phys., 14(20), 11149–11164, doi:10.5194/acp-14-11149-2014, 2014.

APPENDIX

Table 5. Refined list from Violetov et al., 2020, for Oil and Gas point sources, sorted by their calculated emission load as seen by TROPOMI/S5P for the year 04.2018-03.2019.

LATITUDE	LONGITUDE	NAME	COUNTRY	EMISSIONS (kt[SO2]/yr)	UNCERTAINTIES
27.55	52.56	Zagroz	Iran	695	41.3
19.4	-92.24	Cantarell	Mexico	452	27.4
17.89	-93.19	Reforma	Mexico	439	27
25.15	52.88	Das Island	United Arab Emirates	405	24.7
28.5	49.8	Fereidoon	Saudi Arabia	360	22.4
29.22	50.32	Khark Island	Iran	323	19.9
39.19	65.29	Mubarek	Uzbekistan	236	14.3
22.33	69.75	Essar	India	182	11.6
21.44	39.18	Jeddah	Saudi Arabia	180	11.3
32.5	47.21	Dehloran	Iran	178	10.9
20.05	-99.28	Tula	Mexico	162	10.1
31.29	49.12	Ahvaz	Iran	160	9.8
23.95	38.31	Yanbu	Saudi Arabia	155	9.9
36.47	60.85	Khangiran	Iran	152	9.4
10.08	-64.87	Jose	Venezuela	146	10.8
46.77	48.12	Astrakhan	Russia	138	10.4
27.07	49.57	Jubail	Saudi Arabia	137	9.1
16.21	-95.18	Salina Cruz	Mexico	117	8.8
51.87	54.76	Orenburg	Russia	115	9.9
33.49	44.35	Bagdad	Iraq	114	7.2
24.9	51.55	Mesaieed	Qatar	102	7
23.85	53.65	Habshan	United Arab Emirates	102	6.7

Table 6 Refined list from Violetov et al., 2020, for Power Plant point sources, sorted by their calculated emission load as seen by TROPOMI/S5P for the year 04.2018-03.2019.

LATITUDE	LONGITUDE	NAME	COUNTRY	EMISSIONS (kt[SO2]/yr)	UNCERTAINTIES
-26.25	29.18	Kriel	South Africa	582	34.4
22.67	39.03	Rabigh	Saudi Arabia	437	26.2
24.09	82.68	Vindhyachal	India	425	25.3
-23.71	27.56	Matimba	South Africa	331	19.7
11.55	79.44	Neyveli	India	299	18.2
20.63	39.56	Shaiba	Saudi Arabia	276	16.7
29.36	47.79	Al Doha	Kuwait	273	16.3
22.39	82.74	Korba	India	264	15.8
42.15	26	Marica	Bulgaria	256	16.4
38.35	36.98	Afsin Elbistan	Turkey	256	15.5

21.1	85.08	Talcher	India	252	15.4
21.78	84.06	Sterlite	India	249	15.1
37.03	27.9	Kemerkoy	Turkey	233	15
47.99	37.24	Kurakhovskaya	Ukraine	209	14.2
-26.74	27.98	Lethabo	South Africa	208	12.6
44.67	20.16	Nikola Tesla	Serbia	206	13.8
44.52	18.6	Tuzla	Bosnia and Herzegovina	196	13.3
-27.1	29.77	Majuba	South Africa	194	12
23.66	68.78	Kutch	India	190	11.7
13.25	80.33	North Chennai	India	180	11.7
17.6	83.09	Simhadri	India	174	11.4
48.46	38.21	Vuglegirska	Ukraine	174	12.6
20.01	79.29	Chandrapur	India	171	10.5
18.75	79.46	Ramagundam	India	158	9.9
17.98	-102.12	Petacalco	Mexico	154	11.8
52.12	76.87	Pavlodar	Kazakhstan	153	11.7
57.11	61.7	Reftinskaya	Russia	137	13.1
39.57	29.88	Seyitomer	Turkey	133	9.3
21.25	79.1	Koradi	India	128	8.2
23.58	87.21	Durgapur	India	127	8.4
27.15	56.12	Bandar Abbas	Iran	125	8.1
-5.89	106.03	Suralaya	Indonesia	121	8.5
21.02	-97.33	Tuxpan	Mexico	121	8.8
-38.25	146.57	Loy Yang	Australia	120	10.8
23.07	-81.54	Guiteras	Cuba	117	8.1
17.62	80.7	Kothagudem	India	113	7.7
39.08	37.3	Kangal	Turkey	108	7.4
47.4	40.23	Novocherkassk	Russia	105	9.6
21.93	83.34	Raigarh Mill	India	102	6.8

Table 7. Refined list from Violetov et al., 2020, for Smelter point sources, sorted by their calculated emission load as seen by TROPOMI/S5P for the year 04.2018-03.2019

LATITUDE	LONGITUDE	NAME	COUNTRY	EMISSIONS (kt[SO2]/yr)	UNCERTAINTIES
69.36	88.13	Norilsk	Russia	1636	97.2
29.98	55.86	Sarcheshmeh	Iran	286	17
-20.73	139.48	Mt Isa	Australia	246	15
58.35	60.07	Krasnouralsk	Russia	153	12.9
40.86	69.53	Almalyk	Uzbekistan	123	8
46.83	74.94	Balqash	Kazakhstan	116	8
57.41	60.08	Kirovograd	Russia	112	11.4

Table 8. Refined list from Violetov et al., 2020, for Volcanic point sources, sorted by their calculated emission load as seen by TROPOMI/S5P for the year 04.2018-03.2019

LATITUDE	LONGITUDE	NAME	COUNTRY	EMISSIONS (kt[SO2]/yr)	UNCERTAINTIES
-16.25	168.12	Ambrym	Vanuatu	1458	86.7
37.73	15	Mt. Etna	Italy	865	51.3
-15.4	167.83	Aoba	Vanuatu	745	45.2
1.68	127.88	Dukono	Indonesia	738	44
-19.53	169.44	Yasur	Vanuatu	655	39.3
19.42	-155.29	Kilauea	USA	562	35.3
31.59	130.66	Sakura-jima	Japan	541	32.6
-6.14	155.2	Bagana	Papua New Guinea	499	30
4.9	-75.32	Nevado del Ruiz	Colombia	488	29.9
11.98	-86.16	Masaya	Nicaragua	398	24.3
13.26	123.69	Mayon	Philippines	372	22.3
10.03	-83.77	Turrialba	Costa Rica	358	22.1
19.02	-98.62	Popocatepetl	Mexico	357	21.2
-1.41	29.2	Nyamuragira	Democratic Republic of Congo	344	20.6
-15.8	-71.86	Sabancaya	Peru	335	20.2
30.79	130.31	Kikai	Japan	308	19.1
-7.94	112.95	Tengger Caldera	Indonesia	289	17.4
50.33	155.46	Chikurachki	Russia	273	18
-8.51	124.13	Sirung	Indonesia	270	16.4
-37.52	177.18	White Island	New Zealand	268	17.5
-4.08	145.04	Manam	Papua New Guinea	266	16.1
56.64	161.34	Shiveluch	Russia	225	14.4
-5.53	148.42	Langila	Papua New Guinea	201	12.8
52.45	158.2	Mutnovsky	Russia	197	13.8
29.64	129.72	Suwanose-jima	Japan	191	12.3
56.17	-159.38	Veniaminof	USA	189	14.7
32.88	131.11	Aso	Japan	185	13.2
2.78	125.4	Karangetang	Indonesia	181	11
10.41	123.13	Kanlaon	Philippines	180	11.6
-21.23	55.71	Reunuin	Reunion Island, France	167	10.7
43.42	142.69	Tokachi	Japan	157	14
-6.11	105.42	Krakatau	Indonesia	147	9.8
14.47	-90.88	Fuego	Guatemala	141	8.7
12.7	-87	San Cristobal	Nicaragua	141	9.2
-37.86	-71.16	Copahue	Argentina	139	8.9
13.6	40.67	Erta Ale	Ethiopia	130	8

-1.7	101.26	Kerinci	Indonesia		128	8.2
54.05	159.45	Karymsky	Russia		124	10.9
-5.05	151.33	Ulawun	Papua New Guinea		118	7.7
-8.06	114.24	Ijen	Indonesia		107	6.9
56.06	160.64	Kliuchevskoi	Russia		105	7.7
16.72	-62.18	Soufriere Hills	Montserrat (UK)		102	7.4
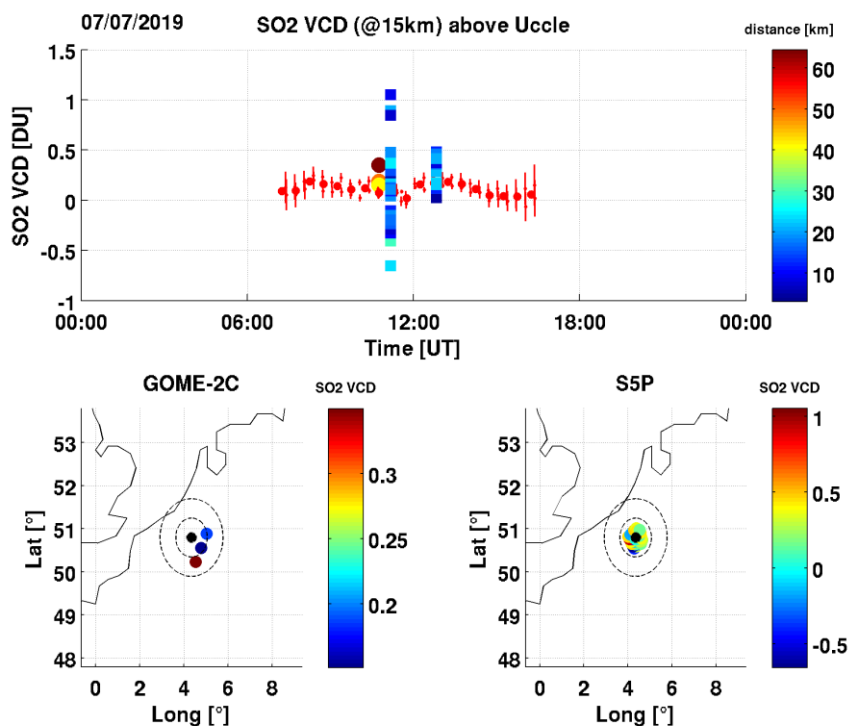
Figure S 1. As Figure 30, for Uccle on the 7th of July 2019.
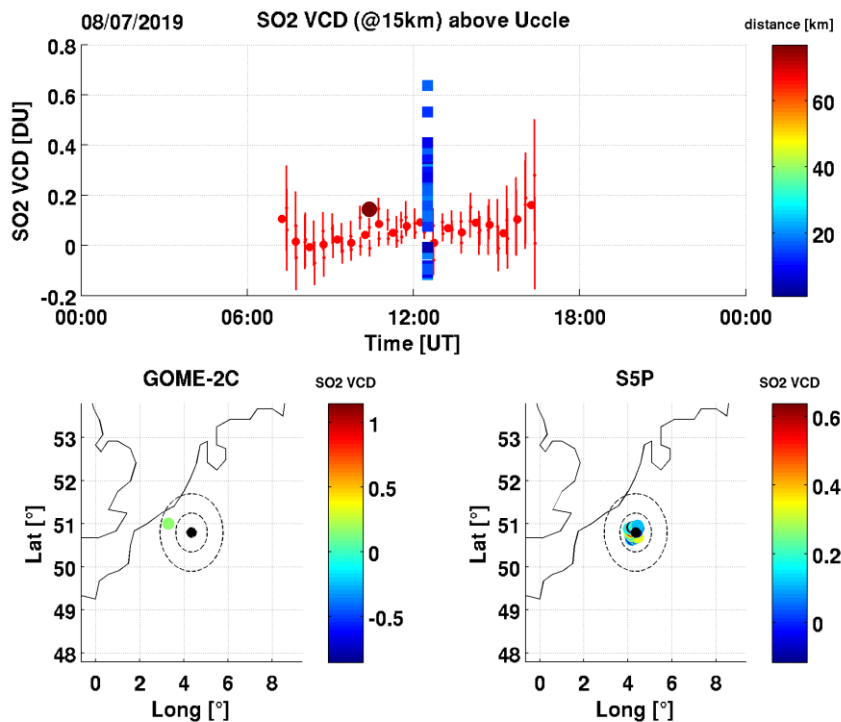
Figure S 2. As Figure 30, for Uccle on the 8th of July 2019.
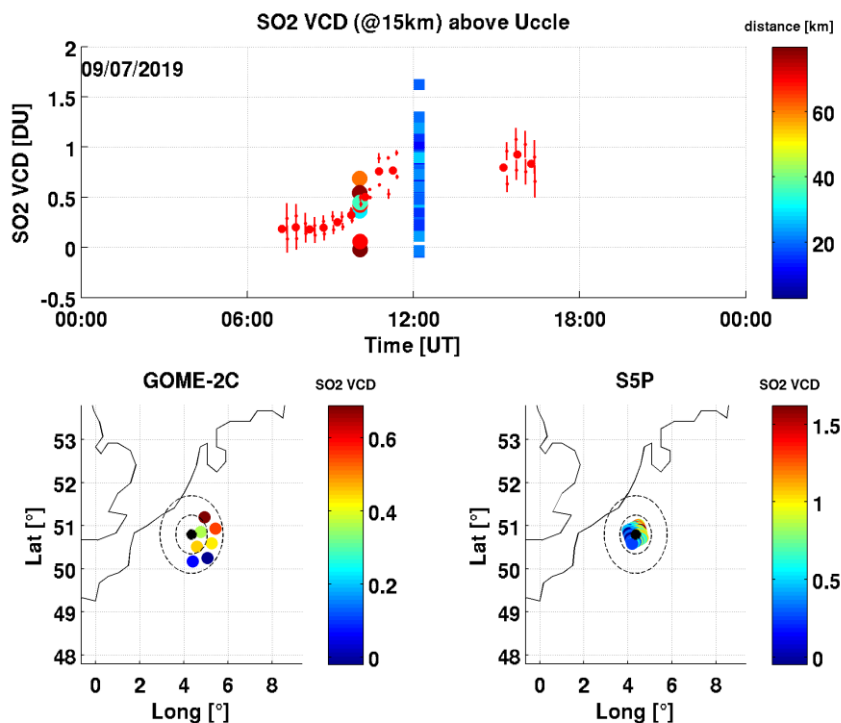
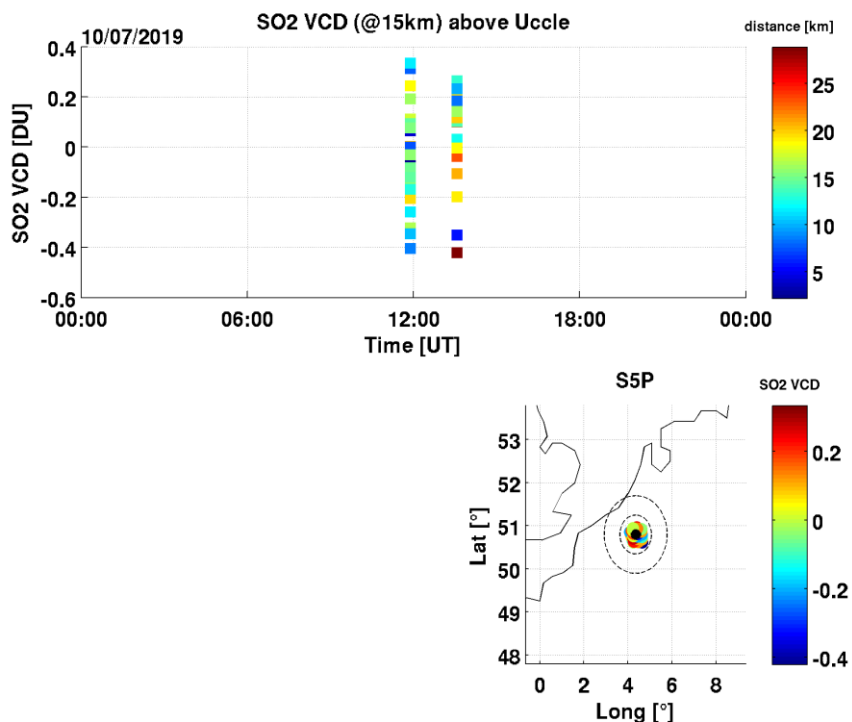Figure S 3. As Figure 30, for Uccle on the 9th of July 2019.

Figure S 4. As Figure 30, for Uccle on the 10th of July 2019.
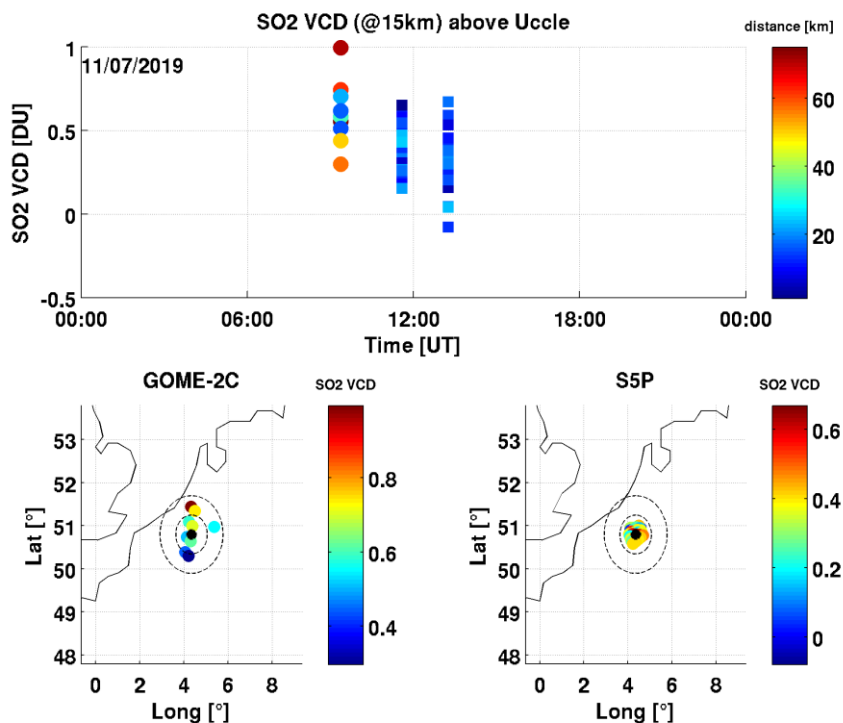

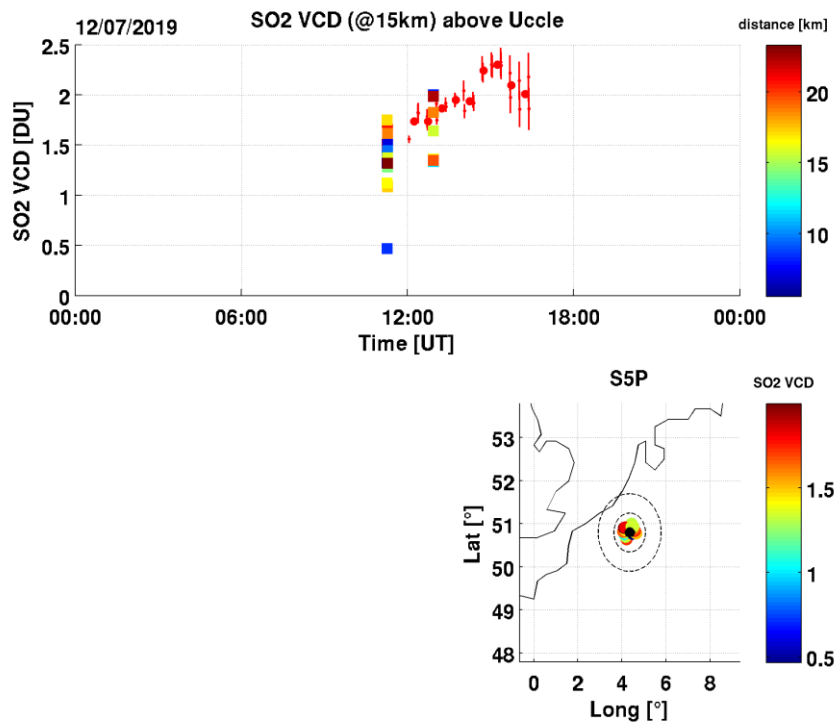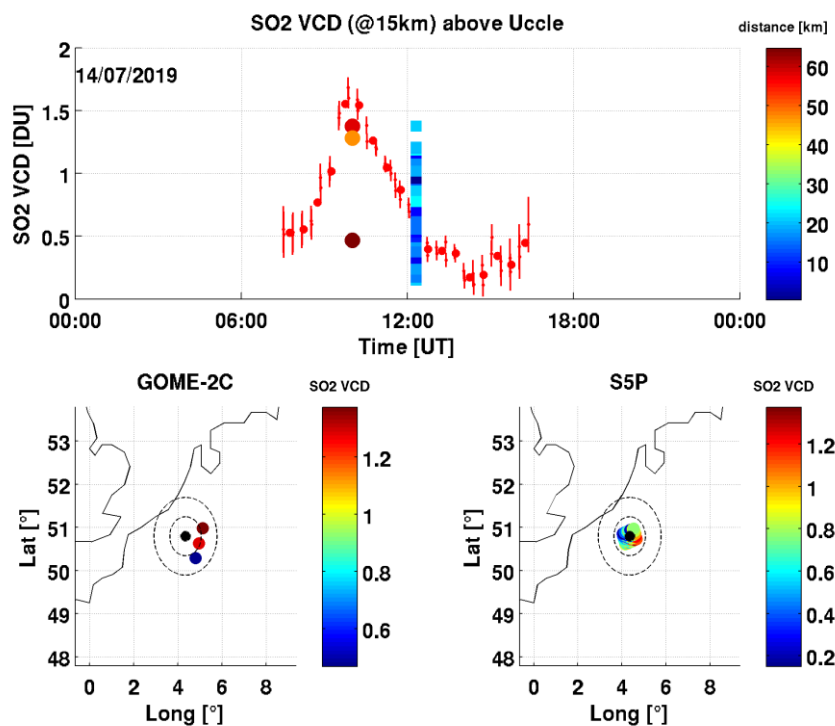Figure S 5. As Figure 30, for Uccle on the 11th of July 2019.

EUMETSAT
AC SAF

REFERENCE: **SAF/AC/AUTH/VR/SO2**
ISSUE: 11/2020
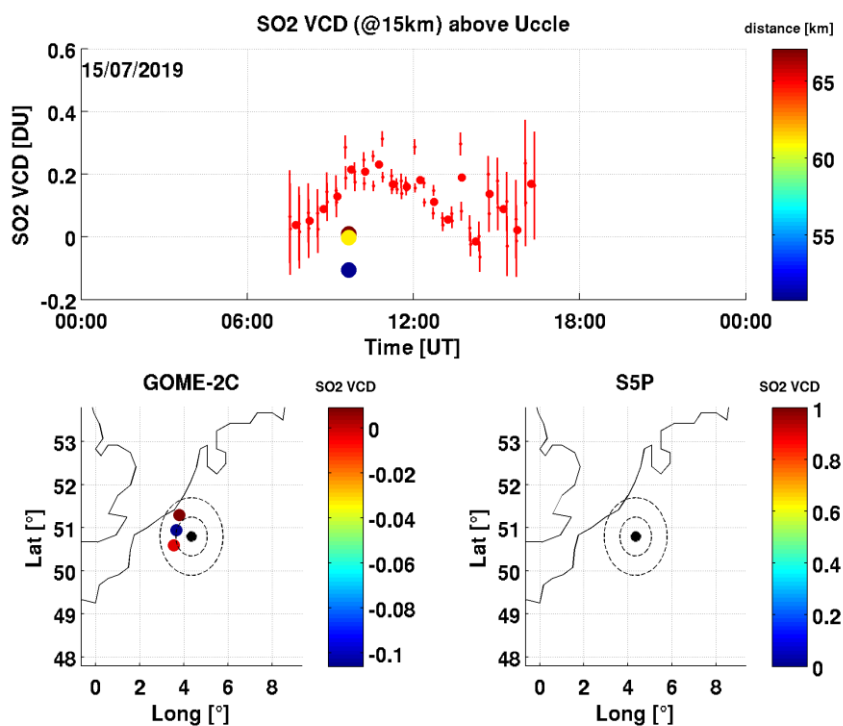DATE: 30/11/2010
PAGES: Page **61** of **62**

Figure S 6. As Figure 30, for Uccle on the 12th of July 2019.

Figure S 7. As Figure 30, for Uccle on the 14th of July 2019.

Figure S 8. As Figure 30, for Uccle on the 15th of July 2019.